

# Asynchronous Data Fusion With Randomly Delayed Measurements for Lane-Level Vehicle Tracking in Tunnel Environment

Guoqiang Mao<sup>1</sup>, Fellow, IEEE, Tianxuan Fu<sup>1</sup>, Xiaojiang Ren<sup>1</sup>, Member, IEEE,  
Keyin Wang<sup>1</sup>, Graduate Student Member, IEEE, Zhaozhong Zhang,  
Zhong Wu, and Dahai Xu

**Abstract**—Sensor fusion plays an increasingly important role in real-time traffic perception using roadside sensing devices because the use of single type of sensors often fail to deliver satisfactory performance in certain harsh environment. This paper investigates asynchronous data fusion for lane-level vehicle tracking with randomly delayed measurements and inaccurate detections from millimeter wave (MMW) radars and magnetic sensors in tunnels, where vehicle tracking with single type of sensors can not meet the requirements of reliable and accurate lane-level tracking due to inaccurate radar detections at far distances, noisy radar detections in tunnel environment, and missed or false vehicle detections by magnetic sensors. A multisensor data association algorithm is first designed to assign the measurements of MMW radar and magnetic sensors to a particular vehicle. A multi-lane estimation model is then developed, which employs Bayesian weight mixture filtering to fuse MMW radar and magnetic sensor measurements and to estimate the lane in which a vehicle is located. Finally, the proposed algorithm is implemented in a real environment - the Xianfengding Tunnel located in Jiangxi Province, China. Experiments are conducted to validate the accuracy of the proposed method using real data. The proposed method and the collected data are further integrated to establish a real-time digital twin system aimed at supporting advanced traffic management. The fusion results and the real radar measurement dataset of the tunnel are made available at <https://github.com/futianxuan/data>.

**Index Terms**—Asynchronous data fusion, roadside sensor, MMW radar, magnetic sensor, lane-level vehicle tracking.

## I. INTRODUCTION

**R**OADSIDE perception is important for establishing a traffic digital twin system supporting advanced traffic

Received 30 June 2024; revised 17 November 2024 and 20 January 2025; accepted 11 March 2025. This work was supported by the National Natural Science Foundation of China under Grant U21A20446. The Associate Editor for this article was C. Lv. (Corresponding author: Tianxuan Fu.)

Guoqiang Mao is with the School of Transportation, Southeast University, Nanjing 211189, China (e-mail: g.mao@ieee.org).

Tianxuan Fu and Keyin Wang are with the Smart Transportation Institute and the School of Telecommunications Engineering, Xidian University, Xi'an 710071, China (e-mail: futianxuan@stu.xidian.edu.cn; keyinwang@stu.xidian.edu.cn).

Xiaojiang Ren is with the Smart Transportation Institute and Guangzhou Research Institute, Xidian University, Xi'an 710071, China (e-mail: xjren@xidian.edu.cn).

Zhaozhong Zhang is with the School of Information Engineering, Nanchang Hangkong University, Nanchang 330000, China (e-mail: 71033@nchu.edu.cn).

Zhong Wu and Dahai Xu are with Jiangxi Fangxing Technology Company Ltd., Nanchang 330009, China (e-mail: 66397942@qq.com; 957002527@qq.com).

Digital Object Identifier 10.1109/TITS.2025.3551353

management and facilitating the future mass deployment of Connected Automated Vehicles (CAVs) via road-vehicle collaborations [1], [2], [3], [4], [5]. Roadside perception systems support advanced traffic management by providing real-time data for traffic flow optimization and vehicle tracking. Continuous monitoring and relaying of traffic conditions to management centers facilitate smoother traffic movements and improve overall road traffic safety. Sensors strategically placed along the roadside detect vehicles in real-time and promptly transmit the detection results to CAVs with short latency via vehicle-to-infrastructure (V2I) communications [1], [6]. Roadside perception can complement the CAVs' on-board perception, providing a more comprehensive field of view, fewer occluded objects, and more accurate perception than on-board sensing alone, especially in complicated scenarios, beyond-line-of-sight environment, harsh weather and poor lighting conditions [7]. These roadside sensors can further alleviate the sensing requirements of CAVs' on-board sensors, thereby reducing the cost of CAVs and making them more affordable. The development of cooperative vehicle-infrastructure systems also requires high-quality perception data from roadside sensors to ensure safe and efficient traffic operation [8]. Therefore, there is an urgent need to effectively utilize existing roadside sensing devices or deploy new sensors to enhance the accuracy of roadside perception.

Sensing methods that rely on the single type of sensors to obtain target motion information tend to produce incomplete and inaccurate data in dynamic and complex environment [9]. Many traffic monitoring techniques using roadside sensors have been introduced and studied [10], [11], [12]. As the most commonly used roadside sensor, cameras primarily rely on artificial intelligence-driven object detection algorithms for perception. Cameras can obtain rich information from images, but the shortcomings of video-based detection are also obvious. Poor illumination conditions at night or in tunnels and local feature occlusion significantly affect the detection accuracy and the continuity of vehicle trajectories [12]. LiDAR is another popularly used sensor. It has a greater detection distance than that of a camera, and its perception information is more comprehensive [13]. However, LiDAR requires significant computing power and storage capacity to process the large amount of point cloud data being produced. Its detection results are susceptible to interference from airborne particles [14], and the price of LiDAR is generally very high.

MMW radar is highly sensitive to object's velocity and has been extensively used in practical applications, which provides a cost-effective alternative to LiDAR [4]. The MMW radar is almost unaffected by environmental factors and is robust for the detection of partially occluded objects. However, the MMW radar detection range is limited, generally not more than 300 m, and larger vehicles close to the radar are prone to being detected as two or more objects [15]. Additionally, the lateral detection accuracy of MMW radar will decrease significantly as the detection distance increases. In some harsh environment such as a tunnel, MMW radar detection is also prone to multi-path interference and noise. A critical challenge of roadside perception is therefore the optimum trade-off between cost and accuracy. In this paper, we focus on the cost-effective and accurate roadside perception using a fusion of MMW radars and magnetic sensors.

Magnetic sensors have been extensively used for road traffic detection [2], [16], [17], [18], [19]. In our previous works, we embed magnetic sensors into a new type of Internet of Things (IoT) device [20]. Specifically, we for the first time report on the design of small and powerful, ubiquitously deployed, solar-powered, road-embedded plug-and-play IoT devices that can be integrated with multiple sensors such as temperature, humidity, light, vibration and magnetic sensors, LED lights, termed smart studs [1]. The main detection information provided by a smart stud with a magnetic sensor includes the measurement timestamps of passing vehicles and the deployment location of the magnetic sensor. Furthermore, as magnetic sensors can only detect close-by vehicles, the event that a vehicle is detected by a magnetic sensor also suggests that the vehicle is in a lane adjacent to the magnetic sensor. Hence magnetic sensors can provide lane information of a vehicle. Armed with sophisticated data association and tracking algorithms, collectively, smart studs with magnetic sensors are strategically deployed along the lane boundary lines to achieve the perception of vehicle lane-level information, including position, speed, and vehicle type [20]. Magnetic sensors have the advantages of being robust to weather changes and are unaffected by multi-path interference, which complement MMW radars, especially in tunnel environment. However, as the local magnetic field generated by a target attenuates quickly with the propagation distance, magnetic sensors are generally only capable of lane-level detection - they cannot detect targets too far away. On the other hand, MMW-based detection is generally more accurate than magnetic sensors but suffers from occlusion and multi-path interference, which often causes "ghost" detection in tunnel environment, and that the radial detection accuracy degrades quickly with an increase in detection distance. The complementary nature of MMW radar and magnetic sensors, especially in tunnel environment, motivates us to create a robust detection system fusing the measurements of both sensors.

Multi-sensor fusion (MSF) methods for asynchronous sensors are typically categorized into centralized and distributed strategies. Centralized fusion involves transmitting measurement data from different sensors to a fusion center for processing [21]. Centralized fusion, particularly measurement

augmentation techniques based on the centralized Kalman filter [22], is considered optimal, but it requires substantial computational resources due to high-dimensional matrix operations. Therefore, a credibility measure was proposed in [23], which is combined with KF and used to determine whether the delayed measurement is normal or faulty. Besides, reference [24] proposed using least-squares estimation to align measurements between sensors, assuming a constant velocity (CV) model. However, deviations from this assumption can result in model mismatches. To enhance robustness against model uncertainties, an adaptive Kalman filter (AKF) was proposed in [9] and [25], which dynamically adjusts the Kalman gain based on sensor measurement quality, thereby compensating for measurement noise errors. In contrast, distributed fusion involves individual sensors generating local state estimates from their own measurements and transmitting them to the fusion center, which then combines these estimates to produce a globally optimal state estimate according to predefined fusion criteria [26], making it preferable when communication resources are limited [27]. The asynchronous information fusion (AIF) problem for a camera and radar in an intelligent driving system is addressed in [28], where a matrix-weighted fusion algorithm is used to offer a wide detection range and provide reliable fused estimates. Furthermore, a distributed covariance intersection (CI) fusion method was proposed in [29] to fuse estimates in a distributed manner.

Timestamped data from heterogeneous sensors are often asynchronous in nature. Therefore, asynchronous data fusion becomes an important research issue in roadside traffic perception. The basic goal of multi-source data fusion is to obtain more diverse information, hence more robust estimation, than any single type of sensor data [8]. State estimation is a key part of data fusion, which makes full use of prior information and observation information to timely determine the unknown state (such as position, speed, etc.) of the dynamic targets. Many existing methods are designed assuming that all sensors have uniform sampling intervals [30], [31]. For integrated systems with heterogeneous sensor and non-uniform sampling periods, this assumption may be too optimistic [22]. On one hand, many estimation systems employ a periodic estimation and update mechanism, where estimation tasks are executed periodically [32]. On the other hand, in an event-triggered estimation system, the execution of the estimation task is triggered by specific events such as the arrival of new measurements etc., taking into account the communication and computing resource constraints [7]. This usually leads to aperiodic execution of the estimation task. Sampling and estimation may therefore be executed asynchronously [33], which adds difficulty to the design of the estimator. Moreover, due to communication and computing limitations, potential sensor failures and aperiodic execution of the estimation task, there may be multiple measurements arriving within an estimation time interval [34]. Accordingly, a challenging problem arises in multi-source data fusion as to how to make full use the multiple measurements within an estimation interval to design an optimal estimator. A straightforward approach is to utilize only the most recent measurement and discard the others. This approach is however inefficient as much useful information is

lost. For such asynchronous, randomly delayed measurements (due to unreliable and limited communication resources) and aperiodic estimation task execution, data fusion becomes more challenging.

Motivated by the above discussions, in this paper, we consider asynchronous data fusion containing aperiodic and delayed measurements that may temper the performance of vehicle tracking, leading to false lane estimation for lane-level tracking in tunnel. An aperiodic linear estimator is developed based on the backward model [35] to address the challenge of asynchronous fusion with randomly delayed measurements. Furthermore, an accurate and effective lane estimation algorithm based on Bayesian weight mixture is proposed that fully utilizes the complementary advantages of magnetic sensors and MMW radar to determine the lane in which a vehicle is located, especially when measurements from MMW radars and magnetic sensors are inaccurate or missing. Moreover, the above fusion estimator with asynchronous sensors is constructed based on matching the MMW radar and magnetic sensor measurements to the vehicles, achieved through multisensor data association using Hungarian and auction algorithms respectively. To the best of our knowledge, this is the first work that takes delayed, aperiodic and inaccurate measurements into consideration when asynchronously fusing MMW radar and magnetic sensors for accurate lane-level vehicle tracking in a multiple-lane tunnel scenario. Our results shed insight into the design of an asynchronous data fusion algorithm for accurate and robust lane-level vehicle tracking. The vehicle tracking algorithm that fuses MMW radar and magnetic sensors is implemented in a real tunnel environment and forms the core of a traffic digital twin system.

The novelty and major contributions of this paper are summarized as follows:

- 1) An asynchronous data fusion algorithm is developed for accurate lane-level vehicle tracking in tunnel environment fusing randomly delayed and heterogeneous measurements from MMW radars and magnetic sensors. A backward model and a finite-length buffer are employed to address the issue of asynchronous fusion with randomly delayed measurements. Meanwhile, a multisensor association algorithm is designed to match the measurements of MMW radars and magnetic sensors with vehicles.
- 2) Considering that the lateral detection accuracy of MMW radar will deteriorate as the detection distance increases, and missed or false vehicle detections of magnetic sensors, a method based on Bayesian weight mixture of MMW radar and magnetic sensor measurements is proposed to estimate the lane where the vehicle is located and achieve accurate lane-level vehicle tracking.
- 3) The proposed method is validated and evaluated using measurements from the Xianfengding Tunnel and is applied to establish a tunnel traffic digital twin system. The feasibility and effectiveness of our approach are demonstrated through comparisons with vehicle information captured by actual video. Furthermore, the performance of the algorithm is analyzed using both real measurements and simulation data.

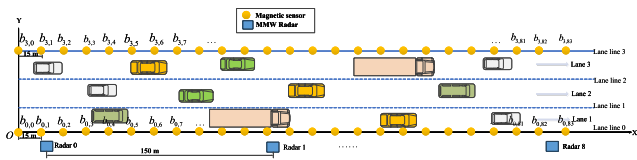


Fig. 1. A schematic diagram of the deployment of magnetic sensors and MMW radars in a three-lane tunnel.

The rest of this article is organized as follows. In Section II, the problem is formulated. Section III presents an optimal state estimation algorithm. Section IV provides an accurate lateral lane-level estimate of the lane in which the vehicle is located. In Section V, the performance of the algorithm is analyzed through simulation and implementation in real tunnel scenarios. Section VI draws the conclusions.

## II. PROBLEM FORMULATION

The schematic diagram and deployment of the MMW radars and magnetic sensors in tunnel are illustrated in Fig. 1. A one-way three-lane tunnel is considered, which is typical in China. The proposed technique can however be readily extended to a tunnel with fewer or more lanes. Each lane has a width  $L = 3.75 m$ , and is numbered  $\Omega = \{1, 2, 3\}$  from right to left, in the vehicle's driving direction. The lane boundary lines are numbered as  $\{0, 1, 2, 3\}$ , denoted by  $\mathcal{O} = \{0, 1, 2, 3\}$ , as shown in Fig. 1. We define the origin as the midpoint of the first magnetic sensor on the rightmost lane line in the driving direction. The  $x$ -axis aligns with the center line of the rightmost lane boundary line, while the  $y$ -axis is locally perpendicular to the  $x$ -axis and points towards the direction of the leftmost lane. In this paper, a curvilinear coordinate system [36] is adopted where the  $x$ -axis may be a curve. The curvilinear coordinate system helps to maximally utilize the knowledge that vehicles in most cases drive inside a lane, which can greatly simplify the estimation problem. The conversion from the curvilinear coordinate system to a global coordinate system can be readily done [37].

Magnetic sensors are positioned along the lane boundary lines at equal distance intervals of  $L_a$  ( $L_a = 15 m$ ) on both sides of the roadway, i.e., on the lane boundary lines 0 and 3 only. Let  $b_{0,j}$  and  $b_{3,j}$  represent the  $j$ -th magnetic sensors positioned on lane boundary lines 0 and 3, respectively. There are no magnetic sensors deployed along the lane boundary lines of the middle lane because of the difficulty to supply electricity to smart studs installed near the middle lane and that solar energy is unavailable in tunnel environment. MMW radars are deployed at equal distance intervals of  $L_b$  ( $L_b = 150 m$ ) along the tunnel wall adjacent to Lane 1 and at a height of 4.5 meters.

Measurements collected by the MMW radar are presented in Table I. Note that  $x$  and  $y$  are the positions in portrait and lateral directions, respectively,  $v_x$  and  $v_y$  are the velocities in portrait and lateral directions, respectively, in the radar's local coordinate system. The MMW radar data mainly contain timestamped vehicle position and velocity information. Measurements collected by the magnetic sensor are presented

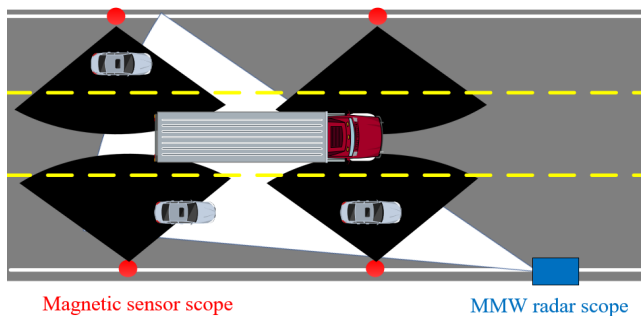


Fig. 2. An illustration of the different detection ranges of MMW radars and magnetic sensors.

TABLE I  
COLLECTED DATA FROM THE MMW RADAR

Sensor	Timestamp(s)	$x(m)$	$y(m)$	$v_x(m/s)$	$v_y(m/s)$
MMW radar	42.073	101.037	9.118	18.492	0.570
MMW radar	42.194	103.261	9.095	18.492	0.161
MMW radar	42.313	105.320	9.085	18.492	0.133

TABLE II  
COLLECTED DATA FROM MAGNETIC SENSOR

Sensor	Timestamp(s)	$x(m)$	Lane line
magnetic sensor	49.977	15	0
magnetic sensor	51.077	30	0
magnetic sensor	52.073	45	3

in Table II. The magnetic sensor data contain the measurement timestamp and the location of the magnetic sensor in the aforementioned curvilinear coordinate system. Magnetic sensor measurement is triggered by the passing vehicle. Let  $e_{0,k}^j$  and  $e_{3,k}^j$  represent the vehicle detection events of magnetic sensors  $b_{0,j}$  and  $b_{3,j}$  at time  $t_k$  respectively where  $e_{0,k}^j = 1$  ( $e_{3,k}^j = 1$ ) means successful detection and  $e_{0,k}^j = 0$  ( $e_{3,k}^j = 0$ ) means no detection. As mentioned earlier, magnetic sensors can only detect close-by vehicles. Therefore,  $e_{0,k}^j = 1$  ( $e_{3,k}^j = 1$ ) also conveys the information that *with a high chance*, the vehicle is located in lane 1 (lane 3). It is worth mentioning that there are also exceptions in the detection of magnetic sensors. For example, a large vehicle (hence with more ferromagnetic material) driving in the middle lane may also trigger the detection of a magnetic sensor located in lane line 0 (see Fig. 1). This situation must be considered in the estimation of vehicle lane. When a vehicle passes the magnetic sensors, measurement timestamps, the lateral positions and lane line information of magnetic sensors being triggered are transmitted to the fusion center via a low-rate wireless LoRA transmission, a wireless transmission technique designed for IoT applications, at a non-periodic sampling rate. MMW radar detects the position and speed of the vehicle at a periodic sampling rate. Due to the large amount of data produced by MMW radars, MMW radars are connected to the fusion center via optical fibers. Hence, the data from the MMW radars and the magnetic sensors arrive at the fusion center with vastly different delays and loss rate. The fusion center conduct the vehicle state estimation using MMW radar and magnetic sensor data every  $T$  ( $T = 0.1$  s) seconds.

As the environment under consideration is a highway or a tunnel, a constant-velocity vehicle motion model is employed to capture the kinematic relationship during a tracking process. A more intricate model, such as a constant acceleration model, has been tried but does not necessarily increase the vehicle tracking accuracy. Specifically, we consider a class of discrete time-varying linear system that evolve from time  $t_{k-1}$  to time  $t_k$  following a linear state space model:

$$x(k) = F(k, k-1)x(k-1) + \omega(k-1) \quad (1)$$

where the vehicle state is represented as  $x(k) = [p_x(k), p_y(k), v_x(k), v_y(k)]^T$ ,  $p_x(k)$  and  $p_y(k)$  are the positions in portrait and lateral directions, respectively,  $v_x(k)$  and  $v_y(k)$  are the velocities. The system noise  $\omega(k-1) = [w_x(k-1), w_y(k-1), w_{v_x}(k-1), w_{v_y}(k-1)]^T$  is a zero-mean white Gaussian noise with a known covariance matrix  $Q$ .  $F(k, k-1)$  is the system transition matrix to  $t_k$  from  $t_{k-1}$ .

$$F(k, k-1) = \begin{bmatrix} 1 & 0 & \Delta t_k & 0 \\ 0 & 1 & 0 & \Delta t_k \\ 0 & 0 & 1 & 0 \\ 0 & 0 & 0 & 1 \end{bmatrix} \quad (2)$$

where  $\Delta t_k = t_k - t_{k-1}$ . Initial vehicle motion information is estimated separately from the MMW radars and magnetic sensors. Note that vehicle information is asynchronously obtained from the MMW radars and magnetic sensors. The MMW radar operates at a constant sampling rate, while the magnetic sensor employs an event-triggered mechanism in which a new measurement is triggered by the detection of a passing vehicle. The measurement equation of magnetic sensors and MMW radars is given by

$$z^i(k) = H^i(k)x(k) + v^i(k), \quad i \in \{r, b\} \quad (3)$$

where  $z^r(k) = [z_x(k), z_y(k), z_{v_x}(k), z_{v_y}(k)]^T$  and  $z^b(k) = [z_x(k)]$  are measurements of MMW radar and magnetic sensors, respectively. Parameter  $H^i(k)$  is a known measurement matrix,  $H^r(k) = \text{diag}[1, 1, 1, 1]$ ,  $H^b(k) = [1, 0, 0, 0]$ ,  $v^i(k)$  is an additive noise, which is a zero-mean white Gaussian noise with a known covariance matrix  $R^i(k)$ . It is assumed that the MMW radar measurement noise and magnetic sensor noise are independent, and the measurement noise  $v^i(k)$  is uncorrelated with process noise  $\omega(k)$ .

Communication delays and measurement losses are almost inevitable in a networked environment and should be considered in the filter design. MMW radars are connected to a fiber-optic transmission system whereas magnetic sensors transmit their data through wireless and low datarate LoRA connections designed specifically for IoT applications. Therefore, transmission delays of magnetic sensors generally are much larger than MMW radar measurements. The MMW radar sampling time is set to be the same as the state update time. The time instant of the  $j$ -th measurement from sensor  $i$ ,  $i \in \{r, b\}$ , received at the fusion center during the interval  $(t_k, t_{k+1}]$  are denoted as  $t_k^{i,j}$ ,  $j = 1, 2, \dots, n$ , and satisfy  $t_k < t_k^{i,1} < t_k^{i,2} < \dots < t_k^{i,n} \leq t_{k+1} = t_k + T$ . Due to aperiodic sampling and network-induced random delays, multiple measurements may be available, or no newly arrived

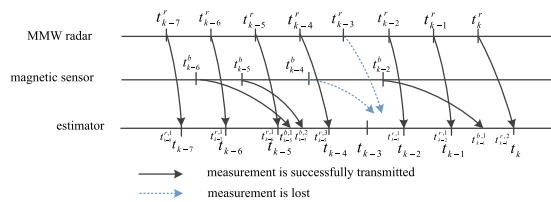


Fig. 3. An illustration of the estimation system with lost and delayed measurements. Parameter  $t_k$  represents the estimator time,  $t_k^r$  ( $t_k^b$ ) is the MMW radar measurement (magnetic sensor measurement) time and  $t_{k-1}^{r,1}$  ( $t_{k-1}^{b,2}$ ) is the time the MMW radar measurement (magnetic sensor measurement) is received at the estimator or the fusion center during  $(t_{k-1}, t_k]$ .

measurement may occur during an estimation interval. Taking the estimation interval  $(t_{k-1}, t_k]$  in Fig. 3 for example, where MMW radar measurement  $z^r(t_k^r)$  and magnetic sensor measurement  $z^b(t_{k-2}^b)$  are received during the state update interval  $(t_{k-1}, t_k]$ . Due to the very small transmission delays of MMW radar measurements, it is often the case that MMW radar measurements are generated and received during the same interval  $(t_{k-1}, t_k]$  whereas magnetic sensor measurement  $z^b(t_{k-2}^b)$  generated during  $(t_{k-3}, t_{k-2}]$  is received during  $(t_{k-1}, t_k]$ . Due to the wireless low datarate LoRA connections used for transmitting magnetic sensor data, measurements from magnetic sensors often suffer from large delays and out-of-sequence arrivals at the fusion center as shown in Fig. 3.

In addition to the vehicle state vector  $x(k) = [p_x(k), p_y(k), v_x(k), v_y(k)]^T$  defined earlier, in this paper, we augment the state vector  $x(k)$  with a further state variable  $\beta_k \in \{1, 2, 3\}$  where  $[\Pr(\beta_k = 1), \Pr(\beta_k = 2), \Pr(\beta_k = 3)]^T$  is the probability that the vehicle is located in lane 1, 2 or 3 respectively. Obviously  $\Pr(\beta_k = 1) + \Pr(\beta_k = 2) + \Pr(\beta_k = 3) = 1$ . Apparently,  $\beta_k$  has some connection with the state variable  $p_y(k)$  but the value of  $\beta_k$  or  $\Pr(\beta_k)$  does not transform directly to the corresponding value of  $p_y(k)$  and the converse. Furthermore, the addition of a separate state variable  $\beta_k$  makes it easier to fuse the measurements of magnetic sensors, which can only be used to roughly indicate the vehicle lane but cannot be directly converted to a continuous measurement value corresponding to  $p_y(k)$ . The update of  $\Pr(\beta_{k+1} = i)$ ,  $i \in \{1, 2, 3\}$  is done separately using a Bayesian procedure, described later in Section IV. Without causing confusion in the expression, we reserve the symbol  $x(k)$  exclusively for  $[p_x(k), p_y(k), v_x(k), v_y(k)]^T$  and consider the lane state vector  $[\Pr(\beta_k = 1), \Pr(\beta_k = 2), \Pr(\beta_k = 3)]$  separately.

The different detection ranges of the magnetic sensor and the MMW radar are illustrated in Fig. 2. In Fig. 2, the black and white fans represent the detection ranges of the magnetic sensor and the MMW radar, respectively. As the detection distance increases, the lateral lane detection resolution of MMW radar decreases. MMW radar may also suffer from inaccurate measurements caused by multipath interference in tunnel environment. On the other hand, magnetic sensors deployed on both sides of the road can detect vehicles in the leftmost and rightmost lanes but may miss vehicles in the middle lane. Note that magnetic sensors and MMW radars have complementary detection range. By fusing the measurements of magnetic sensors and MMW radars, a wide

detection range and robust target tracking can be obtained. The objective of this paper is to design an asynchronous data fusion method with time-varying delays and inaccurate measurements to achieve accurate lane-level vehicle tracking through advantageous combination of MMW radar and magnetic sensors.

### III. DESIGN OF THE LINEAR ESTIMATORS

The following section describes the proposed method for data association and state estimation, which consists of three key components: state prediction, measurement-track association, and vehicle state update. First, state prediction is performed using (4) and (5) in Section III-A. Next, the measurement-track association process associates the MMW radar measurements with the predicted state using (6) to (8), while the magnetic sensor measurements are associated with the predicted state through (9) to (17). Finally, the vehicle state is updated by associated the MMW radar measurements using (21) to (25). The vehicle's longitudinal position is updated separately using the magnetic sensor measurements, as detailed in Section III-C2.

#### A. State Prediction

As a vehicle approaches a tunnel entrance, it is first detected by a MMW radar. Measurements from a radar are first associated with existing active tracks (data association details are outlined in Section III-B). Measurements that fail to associate with existing tracks are used to initialize new targets, with their respective measurements used to initialize the states of the new targets and form new tracks with unique IDs. The motion of the vehicle is modeled as (1). The measurements from the MMW radars and magnetic sensors are fed into the Kalman estimation process through (3). The state prediction is as follows:

$$x(k|k-1) = F(k, k-1)x(k-1|k-1) \quad (4)$$

$$P(k|k-1) = F(k, k-1)P(k-1|k-1)F(k, k-1)^T + Q(k-1) \quad (5)$$

where the state transition matrix  $F(k, k-1)$  is given in (2). The prediction module performs state predictions for all active tracks and brings the states of all active tracks (or vehicles) to the same time  $t_k$ , which is then used for the multisensor association and track update of the next step.

#### B. Measurement-Track Association

Considering the algorithm complexity and the limited computing resources, we design a low computational burden multi-sensor association algorithm by employing a measurement-to-track association. Measurement-to-track association can be divide into two steps: firstly, determining whether the measurement is within the association gate threshold; secondly, calculating the distance between the sensor measurements and the predicted measurement of the track, and then assigning the measurements to the tracks.

1) *Data Association With MMW Radar*: The Mahalanobis distance is used to measure the distance between a MMW radar measurement and the state prediction because it accounts for variable covariances and scale differences. It is particularly suitable for this application because it normalizes the data, providing a consistent way to measure the similarity between the observed measurements and the predicted states. For a MMW radar measurement at time  $t_k$ , the square of the Mahalanobis distance between measurement  $m$  and the corresponding prediction of vehicle  $n$  can be calculated by the following:

$$d_{mn}^2 = (z_m^r(k) - \hat{x}_n(k|k-1))^T S_{mn}(k)^{-1} (z_m^r(k) - \hat{x}_n(k|k-1)) \quad (6)$$

where  $z_m^r(k)$  is the measurement vector of measurement  $m$  from MMW radar, and  $\hat{x}_n(k|k-1)$  is the state prediction vector of the vehicle  $n$ . The measurement covariance is  $S_{mn}(k)$ :

$$S_{mn}(k) = H^r(k)P_n(k|k-1)H^{rT}(k) + R^r(k) \quad (7)$$

where  $R^r(k)$  is the measurement noise covariance matrix, and  $P_n(k|k-1)$  is the covariance of the state prediction of vehicle  $n$ . The Mahalanobis distance values  $d_{mn}$  are recorded in the form of a matrix  $M_{dis}$ : the rows of the matrix  $M_{dis}$  are MMW radar measurements and the columns are the vehicles.

$$M_{dis} = \begin{cases} (d_{mn}^2)_{c \times l}, & \text{if } d_{mn}^2 \leq G \\ d_{max}, & \text{if } d_{mn}^2 > G \end{cases} \quad (8)$$

where subscript  $c$  is the number of sensor measurements,  $l$  is the number of tracks (or vehicles), and  $G$  is the association threshold. Only the measurements within the threshold could be associated.  $d_{max}$  is a large constant, which means the measurement is outside the threshold of the track. Since the square of the Mahalanobis distance obeys the chi-square distribution whose degrees of freedom depend on the dimension of the state vector, the threshold  $G$  can be defined according to the probability table of the chi-square distribution. In this paper, to realize the association of multiple measurements and vehicles, the Hungarian algorithm is used for the optimal assignment due to its efficiency and effectiveness in solving the assignment problem. It guarantees a globally optimal solution with a polynomial time complexity, making it suitable for real-time applications where quick and accurate association of multiple measurements and tracks is essential [38]. Then, measurements that are not associated will initialize new tracks and measurements that are successfully associated will be used to update the vehicles' states.

2) *Data Association With Magnetic Sensor*: As mentioned in Section II, a magnetic sensor measurement is triggered by a passing vehicle and reports the measurement timestamp and the location of the magnetic sensor detecting the vehicle. The association between a magnetic sensor measurement and a vehicle is conducted based on the measurement timestamp, which is elaborated in the following.

Assume that after the estimation time epoch  $t_k$ , a measurement from a magnetic sensor  $j$  is received with a timestamp  $t_j^b$  and the  $x$  coordinate of the magnetic sensor is denoted by  $x_j^b$ . Here we temporarily ignore the impact of the  $y$  coordinate

and the impact of the vehicle lane, i.e., a vehicle is located in a lane not necessarily adjacent to the magnetic sensor  $j$ . We shall explain shortly later how to deal with the impact of the vehicle lane.

Define  $\sigma_{n,x}$  and  $\sigma_{n,v}$  as the standard deviations of the position and velocity estimates of vehicle  $n$  in the  $x$  direction, respectively:

$$\sigma_{n,x} = \sqrt{P_{k|k}(1,1)} \quad (9)$$

$$\sigma_{n,v} = \sqrt{P_{k|k}(3,3)} \quad (10)$$

where  $P_{k|k}$  is the process covariance matrix of vehicle  $n$  at time  $t_k$ .

The estimated time for a vehicle  $n$  to arrive at the magnetic sensor  $j$  is

$$\hat{t}_{j,n} = t_k + \frac{x_j^b - \hat{p}_{x,n}}{\hat{v}_{x,n}} \quad (11)$$

where  $\hat{p}_{x,n}$  and  $\hat{v}_{x,n}$  are the estimated  $x$  coordinate and estimated speed along the  $x$  axis of vehicle  $n$  at time  $t_k$ , respectively. Without causing confusion and for ease of expression, we drop the subscript  $k$  from  $\hat{p}_{x,n}$  and  $\hat{v}_{x,n}$  and assume that the states of all active vehicles have been brought up to time  $t_k$ . Obviously, Equation (11) is an approximation only. Use  $t_{j,n}$ ,  $p_{x,n}$  and  $v_{x,n}$  to denote the true values for  $\hat{t}_{j,n}$ ,  $\hat{p}_{x,n}$  and  $\hat{v}_{x,n}$  respectively. It can be shown that

$$x_j^b = p_{x,n} + \frac{\int_{t_k}^{t_{j,n}} v_{x,n}(t) dt}{t_{j,n} - t_k} (t_{j,n} - t_k) = p_{x,n} + \bar{v}_{j,n} (t_{j,n} - t_k) \quad (12)$$

where  $v_{x,n}(t)$  is the instantaneous speed at time  $t$  and  $\bar{v}_{j,n} \triangleq \frac{\int_{t_k}^{t_{j,n}} v_{x,n}(t) dt}{t_{j,n} - t_k}$  is the time-averaged speed during  $[t_k, t_{j,n})$ . It follows from (12) that a more accurate approximation for  $\hat{t}_{j,n}$  can be obtained from a first-order Taylor expansion:

$$\begin{aligned} \hat{t}_{j,n} &\approx t_k + \frac{x_j^b - \hat{p}_{x,n}}{\bar{v}_{j,n}} \\ &\approx t_k + \frac{x_j^b - \hat{p}_{x,n}}{\hat{v}_{x,n}} - \frac{x_j^b - \hat{p}_{x,n}}{(\hat{v}_{x,n})^2} \Delta v_{x,n} \end{aligned} \quad (13)$$

where  $\Delta v_{x,n} = \bar{v}_{j,n} - \hat{v}_{x,n}$ . It can be further shown that

$$\text{Var} \left( \frac{x_j^b - \hat{p}_{x,n}}{(\hat{v}_{x,n})^2} \Delta v_{x,n} \right) \approx \frac{(\sigma_{n,x})^2 + (\Delta x_{j,n})^2}{(\hat{v}_{x,n})^4} (\sigma_{n,v})^2 \quad (14)$$

where  $\Delta x_{j,n} = x_j^b - \hat{p}_{x,n}$ . Let

$$\sigma_{j,n} = \frac{\sqrt{(\sigma_{j,x})^2 + (\Delta x_{j,n})^2}}{(\hat{v}_{x,n})^2} \sigma_{n,v} \quad (15)$$

Based on the above analysis, we are now ready to present the data association algorithm for magnetic sensor measurement. As introduced before, first an association gate is formed to filter out vehicles that apparently cannot be associated with a measurement. Then, for the multiple-measurement-multiple-vehicle association problem, an auction algorithm is employed to obtain the optimum association due to its efficiency and

robustness, especially when dealing with large numbers of measurements and vehicles.

During the track initialization stage, the estimates of vehicle states may contain large errors. Therefore, it is more prudent to use the maximum and the minimum speed to form the association gate:  $[t_k + \frac{\Delta x_{j,n}}{v_{max}} - \varepsilon_{t,j}, \hat{t}_j + \frac{\Delta x_{j,n}}{v_{min}} + \varepsilon_{t,j}]$ , where  $v_{max}$  and  $v_{min}$  are respectively the maximum and the minimum speeds in a particular environment which can often be empirically determined, e.g., from the speed limit. The term  $\varepsilon_{t,j}$  accounts for the difference between the local time of smart stud  $j$  and the true time. Due to synchronization error, the smart studs may have a time drift of up to 50 ms. When the vehicle state estimates have converged, a much reduced associate gate is used:  $[t_k + \frac{\Delta x_{j,n}}{\hat{v}_{x,n}} - K_n \sigma_{j,n} - \varepsilon_{t,j}, t_k + \frac{\Delta x_{j,n}}{\hat{v}_{x,n}} + K_n \sigma_{j,n} + \varepsilon_{t,j}]$  where  $K_n$  is a value within [2, 10] and is different for each vehicle. Parameter  $K_n$  is first assigned a larger value, e.g., 10. Each successful association with vehicle  $n$  allows us to reduce  $K_n$  a bit (normally by multiplying  $K_n$  by a constant smaller than 1, e.g., 0.9) till the minimum value of 2 is reached. If a vehicle  $n$  is unable to associate with any measurement, then  $K_n$  is multiplied by a constant larger than 1, e.g., 2, until the maximum value of 10 is reached. Such a procedure allows us to just filter in the “right” vehicles to associate with a particular measurement.

If only one vehicle “falls” into the association threshold, that vehicle may be directly assigned to the measurement. However, it is often the case that multiple vehicles may be possibly associated with multiple measurements. In this case, the next step is invoked to resolve the optimum assignment.

For ease of expression, we use  $t_{j,n,min}$  and  $t_{j,n,max}$  to denote the aforementioned minimum and maximum association thresholds. Let  $t_j$  be the measurement timestamp from magnetic sensor  $j$  and let  $\tilde{t}_{j,n} = t_k + \frac{\Delta x_{j,n}}{\hat{v}_{x,n}}$  be the predicted time for vehicle  $n$  to arrive at sensor  $j$  using the state estimates of vehicle  $n$ . The gain of associating measurement from sensor  $j$  to vehicle  $n$  is given by:

$$a_{j,n} = \frac{\max\{(t_j - t_{j,n,min})^2, (t_j - t_{j,n,max})^2\} - (\tilde{t}_{j,n} - t_j)^2}{\sigma_{j,n}} \quad (16)$$

The above gain optimally combines the distances from the association gate boundary and the distance between the predicted arrival time and the actual measurement timestamp, weighed by the uncertainty in vehicle state estimates captured by  $\sigma_{j,n}$ .

The optimum data association problem can then be transformed into the following maximization problem and solved using the auction algorithm [39]:

$$\max \sum_{j,n} I_{j,n} a_{j,n} \quad (17)$$

$$\text{Subject to } I_{j,n} \in \{0, 1\} \quad (18)$$

$$\sum_j I_{j,n} \leq 1, \sum_j I_{j,n} = 1, \text{ when } M \leq N, \quad \forall n \quad (19)$$

$$\sum_n I_{j,n} \leq 1, \sum_i I_{j,n} = 1, \text{ when } N > M, \quad \forall j \quad (20)$$

where  $M, N$  denote the number of measurements and the number of vehicles in the association problem, respectively. Note that only the subset of measurements and the subset of vehicles whose association cannot be resolved using the associate gates (or alternatively, the respective association gates mutually overlap) need to be considered and resolved using the aforementioned maximization problem.

Let us now consider how to incorporate the impact of vehicle lanes in the above data association problem. Consider for example a measurement from sensor  $b_{0,j}$  (see Fig. 1 for an illustration) is received. With a high chance, the measurement may be triggered by a vehicle in Lane 1. However, the situation that the measurement is triggered by a vehicle in Lane 2 or 3 cannot be entirely ruled out because maybe there is a large vehicle driving in Lane 2 or 3. Therefore, with a smaller chance, the measurement may be triggered by a vehicle in Lane 2, and with an even smaller chance, the measurement may be triggered by a vehicle in Lane 3. To capture this effect, a weight is multiplied to the association gain  $a_{j,n}$  in (16). For a vehicle driving in a lane adjacent to the magnetic sensor generating the measurement, a weight of 1 is used. For a vehicle in a lane further away, a weight less than 1 is used.

### C. Vehicle State Update

After the data association problem is resolved, we then consider the update of the vehicle state  $x(k)$  in this subsection and the update of the vehicle lane estimate  $\beta_k$  in Section IV.

1) *Sequential State Update*: After a new measurement is associated with a track, the state update is conducted using (1) and (3) following the standard Kalman update procedure, which is included here for completeness.

$$\hat{x}(k|k-1) = F(k, k-1)\hat{x}(k-1|k-1) \quad (21)$$

$$P(k|k-1) = F(k, k-1)P(k-1|k-1)F(k, k-1)^T + Q(k-1) \quad (22)$$

$$K(k) = P(k|k-1)H^i(k)^T(H^i(k)P(k|k-1)H^i(k)^T + R^i(k))^{-1} \quad (23)$$

$$\hat{x}(k|k) = \hat{x}(k|k-1) + K(k)(z^i(k) - H^i(k)\hat{x}(k|k-1)) \quad (24)$$

$$P(k|k) = P(k|k-1) - K(k)H^i(k)P(k|k-1) \quad (25)$$

where  $i \in \{r, b\}$ .

2) *Out-of-Sequence Update of Randomly Delayed Magnetic Sensor Measurements*: As introduced before, magnetic sensor measurements are transmitted to the fusion center via low data rate LoRA connections and the transmission may incur large delays, e.g., 1-2 s. In comparison, the transmission delays of MMV radar measurements are almost negligible (in the order of milliseconds). Therefore, it happens quite often that a magnetic sensor measurement  $z^b(k)$  with measurement timestamp  $t_k$  arrives after the state has been updated at  $t_k$ , where  $t_k < t_k$ . The current state estimate  $\hat{x}(k)$  needs to

be updated to incorporate this delayed and out-of-sequence magnetic sensor measurement  $z^b(\kappa)$ .

The incorporation of the delayed and out-of-sequence measurement is often done using the backward model and involves the following steps: 1) retrodiction of the state is performed from  $t_k$  to the earlier delayed time  $t_\kappa$ ; 2) the corresponding covariance and filter gain are then computed to update the current state estimate with the delayed measurement  $z^b(\kappa)$  from the magnetic sensor; 3) the state estimate and covariance at  $t_k$  are updated [35]. However, due to modelling error in the target motion model and the uncertain measurement delay, the retrodicted value  $\hat{x}(\kappa|k)$  from  $t_k$  to  $t_\kappa$  may incur a large error, especially when  $t_\kappa$  is much smaller than  $t_k$ . Nowadays, computer storage becomes very cheap and therefore we find it more convenient to store the state estimate and the measurements for a certain amount time where this time threshold, denoted by  $t_{d,max}$ , is set considering LoRA transmission delays. Then, when the measurement  $z^b(\kappa)$  is received, if  $t_\kappa < t_k - t_{d,max}$ , the measurement is discarded as the measurement information may be stale; otherwise, we simply retrieve the state estimate closest to and earlier than  $t_\kappa$ . After analyzing the random LoRA transmission delays of magnetic sensor measurements, the time threshold  $t_{d,max}$  is set to 2 s where  $\sim 95\%$  of magnetic sensor measurements arrive with a delay smaller than or equal to 2 s. Let  $t_{k_{his}}$  be the time instant closest to and earlier than  $t_\kappa$  when the state was updated. The state at time instant  $t_{k_{his}}$  is retrieved. Then all measurements within  $[t_{k_{his}}, t_k]$ , including  $z^b(\kappa)$ , are associated to vehicles and used to update the vehicle states sequentially according to their measurement timestamps following the procedure outline earlier.

#### IV. VEHICLE LANE ESTIMATION

The proposed method for vehicle lane estimation consists of three main steps. First, Bayesian prediction is used to estimate the lane state, as described in (26). Next, lateral measurements from MMW radar and magnetic sensors are combined through a weighted fusion of their probability density functions, producing a fused likelihood function. This fusion process is detailed in (31) to (37) in Section IV-A. Finally, the vehicle's lane is estimated by applying Bayesian updating through (29).

In this section, we consider the vehicle lane estimate. As introduced before, this is done separately from the update of the vehicle state  $x(k)$ . The vehicle lane estimate is conducted following a Bayesian procedure and is updated every  $T$  seconds where  $T = 0.1$  s.

Denote by  $Z_{0:k}$  the set of all measurements received till time  $t_k$  and by  $z_k$  the more recently received measurement. In this paper we use the symbols  $z_k$  and  $z(k)$  interchangeably. Denote by  $\Pr(\beta_k = i|Z_{0:k})$ ,  $i \in \{1, 2, 3\}$  the lane estimate given the measurement set  $Z_{0:k}$ . The lane state prediction can be done using the following equation:

$$\begin{bmatrix} \Pr(\beta_{k+1} = 1|Z_{0:k}) \\ \Pr(\beta_{k+1} = 2|Z_{0:k}) \\ \Pr(\beta_{k+1} = 3|Z_{0:k}) \end{bmatrix} = A_{k+1|k} \begin{bmatrix} \Pr(\beta_k = 1|Z_{0:k}) \\ \Pr(\beta_k = 2|Z_{0:k}) \\ \Pr(\beta_k = 3|Z_{0:k}) \end{bmatrix} \quad (26)$$

where the  $(i, j)$  term of the matrix  $A_{k+1|k}$  represents the probability that the vehicle will change from lane  $i$  to lane

$j$  during time  $T$ :

$$A_{k+1|k} = \begin{bmatrix} 1 - \epsilon & \epsilon & 0 \\ \epsilon & 1 - 2\epsilon & \epsilon \\ 0 & \epsilon & 1 - \epsilon \end{bmatrix} \quad (27)$$

Here,  $\epsilon$  is a small positive constant and is empirically determined based on the probability statistics of actual road vehicles changing lanes. In this paper we set  $\epsilon = 0.1$ . The diagonal elements represent the probabilities of vehicles in lane 1, 2, and 3 staying in their current lanes, respectively.

Now considering a measurement  $z_{k+1}$  is received and assuming that  $z_{k+1}$  and  $Z_{0:k}$  are conditionally independent, it can be readily shown that

$$\Pr(\beta_{k+1} = i|Z_{0:k+1}) = \Pr(\beta_{k+1} = i|Z_{0:k}) \frac{\Pr(\beta_{k+1} = i|z_{k+1})}{\Pr(\beta_{k+1} = i)} \quad (28)$$

where  $\Pr(\beta_{k+1} = i)$  is the prior probability that a randomly chosen vehicle is in Lane  $i$ .  $\Pr(\beta_{k+1} = i)$  can be readily obtained from prior measurement but in practice, we find it suffice to use the approximation that  $\Pr(\beta_{k+1} = 1) = \Pr(\beta_{k+1} = 2) = \Pr(\beta_{k+1} = 3)$  as any inaccuracy in the knowledge of  $\Pr(\beta_{k+1} = i)$  can be compensated by the measurement, i.e., the term  $\Pr(\beta_{k+1} = i|z_{k+1})$ . From (28) and the above discussion, we can get the measurement update equation for  $\Pr(\beta_k = i|Z_{0:k})$ ,  $i \in \{1, 2, 3\}$  as follows:

$$\Pr(\beta_{k+1} = i|Z_{0:k+1}) = C \Pr(\beta_{k+1} = i|Z_{0:k}) \Pr(\beta_{k+1} = i|z_{k+1}) \quad (29)$$

where  $C$  is a normalization constant such that  $\sum_{i \in \{1, 2, 3\}} \Pr(\beta_{k+1} = i|Z_{0:k+1}) = 1$ .

##### A. Measurement Updates for Lane Estimation

Given (29), it remains to determine the value of  $\Pr(\beta_{k+1} = i|z_{k+1})$ , i.e., how the measurements from the MMW radar and the magnetic sensor can be used to estimate the vehicle lane. We separately consider the cases that 1) there is a MMW radar measurement within  $T$ ; 2) there is a magnetic sensor measurement within  $T$  and 3) there are both radar and magnetic sensor measurements within  $T$ . In the last case, an optimum fusion of MMW radar measurement and magnetic sensor measurement is performed.

In the case of a magnetic sensor measurement, assume that a sensor  $b_{0,j}$  reports a vehicle detection event. Denote that event by  $e_{0,j}$  where  $e_{0,j} = 1$  means vehicle detection and  $e_{0,j} = 0$  means no detection. The event that  $e_{0,j} = 1$  means that with a high probability, there is a vehicle in Lane 1, with a small probability, there is a vehicle in Lane 2 and with an even smaller probability, there is a vehicle in Lane 3. Therefore the measurement  $e_{0,j} = 1$  conveys the information that

$$\begin{bmatrix} \Pr(\beta_{k+1} = 1|e_{0,j} = 1) = c_1 \\ \Pr(\beta_{k+1} = 2|e_{0,j} = 1) = c_2 \\ \Pr(\beta_{k+1} = 3|e_{0,j} = 1) = c_3 \end{bmatrix}$$

where  $c_1, c_2, c_3$  are constants such that  $c_1 + c_2 + c_3 = 1$  and  $c_3 < c_2 < c_1$ . The values of  $c_1, c_2$  and  $c_3$  are empirically

chosen based on prior measurements. Other situations such as when sensor  $b_{3,j}$  reports a measurement can be handled analogously. Note that  $e_{0,j} = 1$  suggests that with a high probability, the vehicle is located in Lane 1. On the other hand, no detection, i.e.,  $e_{0,j} = 0$ , is also a strong indicator that with a high probability, the vehicle is *not* in Lane 1.

Now we move on to consider the MMW radar measurement. A MMW radar measures the range  $r$  and the bearing angle  $\theta$  to the vehicle. Many MMW radar manufacturers often convert the MMW radar measurements into a Cartesian coordinate system before output the measurement values in the Cartesian coordinate system. Let  $\delta$  and  $\delta_\theta$  be the standard deviations of the measurements  $r$  and  $\theta$ , respectively. Using the Polar to Cartesian coordinate conversion relationship that  $x_k^r = r \cos \theta$  and  $y_k^r = r \sin \theta$ , it readily follows that the measurement covariance matrix for the radar measurements  $x_k^r$  and  $y_k^r$  are:

$$\begin{bmatrix} r^2 \delta_\theta^2 \sin^2 \theta + \delta^2 \cos^2 \theta & (\delta_\theta^2 - r^2 \delta_\theta^2) \sin \theta \cos \theta \\ (\delta_\theta^2 - r^2 \delta_\theta^2) \sin \theta \cos \theta & r^2 \delta_\theta^2 \cos^2 \theta + \delta^2 \sin^2 \theta \end{bmatrix} \quad (30)$$

As shown in (30), at a small measurement angles  $\theta$ , the measurement error standard deviation in the  $y$ -direction can be approximated by  $\delta_r^2 = r^2 \delta_\theta^2$ , i.e., the measurement error of the MMW radar in the radial direction approximately increases linearly with the distance.

It follows from the above discussion that the pdf of the MMW radar measurement can be approximated by a Gaussian distribution:  $f_r(y) = N(y; y_k^r, \delta_r)$ . The conclusion then readily follows that:

$$\begin{aligned} & \Pr(\beta_{k+1} = 1 | y_{k+1}^r) \\ &= C_r \int_0^L \frac{1}{\sqrt{2\pi} \delta_r} \exp\left(-\frac{1}{2} \left(\frac{y - y_{k+1}^r}{\delta_r}\right)^2\right) dy \end{aligned} \quad (31)$$

$$\begin{aligned} & \Pr(\beta_{k+1} = 2 | y_{k+1}^r) \\ &= C_r \int_L^{2L} \frac{1}{\sqrt{2\pi} \delta_r} \exp\left(-\frac{1}{2} \left(\frac{y - y_{k+1}^r}{\delta_r}\right)^2\right) dy \end{aligned} \quad (32)$$

$$\begin{aligned} & \Pr(\beta_{k+1} = 2 | y_{k+1}^r) \\ &= C_r \int_{2L}^{3L} \frac{1}{\sqrt{2\pi} \delta_r} \exp\left(-\frac{1}{2} \left(\frac{y - y_{k+1}^r}{\delta_r}\right)^2\right) dy \end{aligned} \quad (33)$$

where  $C_r$  is a normalization constant.

1) *Gaussian Mixing for the Fusion of MMW Radar and Magnetic Sensor Measurements*: Now we consider the case that there are both radar and magnetic sensor measurements within  $T$ . In this case, an optimum fusion of the MMW radar and the magnetic sensor measurements is first conducted before the fused measurement is used to update the lane estimate. As the pdf of the lane estimate from the magnetic sensor measurement is discrete while that from the MMW radar is continuous, they are first transformed into the same form.

Let  $u_b(1) = L/2, u_b(2) = 3L/2, u_b(3) = 5L/2$  be respectively the centers of Lane 1, Lane 2 and Lane 3 along the  $y$  axis. The pdf of the lane estimate from the magnetic sensor measurement can be approximated by the following Gaussian mixture function:

$$f_b(y) = c_1 f_1(y) + c_2 f_2(y) + c_3 f_3(y) \quad (34)$$

where  $f_i = N(y; u_b(i), \frac{L}{4})$ . The standard deviation of  $f_i$  is chosen to be  $L/4$ , which implies that with 95% probability, the corresponding  $y$  with pdf  $f_i(y)$  must fall into the region of Lane  $i$  if Lane  $i$  is the estimated lane.

Based on the  $f_r(y)$  and  $f_b(y)$  obtained above, an optimum fusion is obtained through a weighted combination of  $f_r(y)$  and  $f_b(y)$ :

$$f_{\text{fusion}}(y) = \omega_r f_r(y) + \omega_b f_b(y) \quad (35)$$

The optimum weights  $\omega_r$  and  $\omega_b$  are obtained through the following suboptimal constrained maximizing problem [40]:

$$\omega_{\text{subopt}} = \arg \max_w \sum_{i \in \{r,b\}} \omega_i D_{KL}(f_i(y) || f_{\text{fusion}}(y)) \quad (36)$$

where  $D_{KL}(f_i(y) || f_{\text{fusion}}(y))$  is the Kullback-Leibler divergence (KLD) [41] of the two probability density functions  $f_i(y)$  and  $f_{\text{fusion}}(y)$ . This optimization approach is used because the Kullback-Leibler divergence measures the information loss when approximating  $f_{\text{fusion}}(y)$  using the individual distributions  $f_i(y)$ . The derived weights achieve an optimal balance, ensuring  $f_{\text{fusion}}(y)$  effectively integrates essential characteristics of each. The fusion weight determined and proof given in APPENDIX A.

For ease of expression, we use  $z_{k+1}$  to denote the fused measurement. Measurement fusion achieves high robustness and accuracy by reasonably weighting the measurements from different sensors, resulting in more reliable fused measurements. Even if some sensor measurements contain large errors, the optimum fusion can still produce credible posterior estimates. It then follows that

$$\begin{aligned} & \Pr(\beta_{k+1} = i | z_{k+1}) \\ &= C_\beta \int_{(i-1)L}^{iL} f_{\text{fusion}}(y) dy \end{aligned} \quad (37)$$

where  $C_\beta$  is a normalization constant.

## V. EXPERIMENTAL EVALUATION

In this section, we evaluate the effectiveness and performance of the proposed algorithm through both simulations and real-world deployment. Extensive simulations have been conducted to assess the algorithm's efficacy, demonstrating the superiority of the proposed system. The deployment of the algorithm in a real tunnel environment further confirms its accuracy and practical value. The radar measurement data and fusion results are publicly accessible at <https://github.com/futianxuan/data>.

### A. Experimental Platform and Experiment Setup

The proposed system has been deployed in a commercial setting to form part of the advanced traffic and tunnel management system in Xianfengding Tunnel in Jiangxi Province, China, as shown in Fig 4. The three-lane tunnel, spanning approximately 1600 meters, is equipped with nine MMW radars and over 200 magnetic sensors to detect the real-time position of vehicles. MMW radars are deployed at intervals of 150 meters along the tunnel wall and magnetic sensors are

TABLE III  
THE SPECIFIC PARAMETERS OF THE PROCESS NOISE  
COVARIANCE MATRIX

$\sigma_x$	$\sigma_y$	$\sigma_{v_x}$	$\sigma_{v_y}$
$0.75T^2$	$0.45T^2$	$1.5T$	$0.9T$

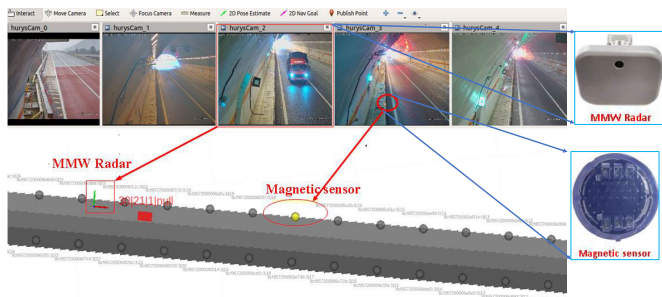


Fig. 4. The actual deployment plan and deployment photos of MMW radars and magnetic sensors in Xianfengding Tunnel, Jiangxi Province, China.

deployed at intervals of 15 meters on both sides of the road lane line. The MMW radars are from Hurys Pty Ltd and with a model number DTAM D39-V.

The initial covariance matrix is established as  $P(0) = \text{diag}[0.01^2, 0.01^2, 0.05^2, 0.01^2]$ . The covariance matrix of the MMW radar measurement noise is primarily determined by errors in transforming radar measurements from polar coordinates to Cartesian coordinates and is set to  $R_r(0) = \text{diag}[0.5^2, 0.7^2, 0.05^2, 0.1^2]$ . The covariance of the measurement noise from the magnetic sensor, considering the ranging error due to timing errors and the geomagnetic measurement error, is  $R_b(0) = 25$ , and the process noise covariance matrix is  $Q_w(k) = \text{diag}[\sigma_x^2, \sigma_y^2, \sigma_{v_x}^2, \sigma_{v_y}^2]$ . The initial process noise covariance matrix is determined through actual system data. These initial values are set following the principles outlined in [42]. The specific parameters involved are shown in Table III.

In the actual deployment, it is difficult to obtain ground truth to gauge the accuracy of the state estimation [43]. Following common practice in the field, we use the normalized innovation as a metric to measure the performance [44]. For example, when considering the horizontal position estimate, denoting the predicted state by  $\hat{p}_{x,n}(k|k-1)$  and the measurement by  $z_{x,n}(k)$  for a vehicle  $n$ , we calculate the normalized innovation of the  $n$ -th object over a time window with  $N_T$  measurements. It is defined as:

$$r_n = \frac{1}{N_T} \sum_k \left( \frac{(\hat{p}_{x,n}(k|k-1) - z_{x,n}(k))^2}{\sigma_{n,x}^2} \right) \quad (38)$$

This value represents the discrepancy between measurement and prediction. This metric is computed first for an object, and averaged in a certain time interval  $T$ . The normalized innovation also employs the covariance matrices considering the predicted position uncertainties,  $\sigma_{n,x}^2$  denote the variance of the prediction position of vehicle  $n$  in  $x$  direction. which is defined as (9).

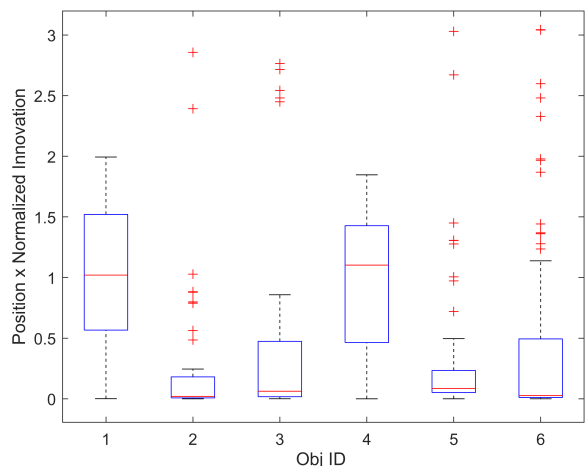


Fig. 5. A boxplot of the normalized innovations for the  $x$ -coordinate after fusing measurements from the MMW radar and magnetic sensors for six randomly chosen vehicles. Both vehicle 1 and vehicle 4, which are in the middle lane and cannot be detected by the magnetic sensor, exhibit higher median values than the other vehicles.

### B. Experimental Evaluation

Fig. 5 and Table IV present the normalized innovations for  $x$  coordinate after fusion of MMW radar and magnetic sensor measurements for six randomly chosen vehicles. The innovations of vehicle 1 and vehicle 4 are larger than those of other vehicles. The reason is that these two vehicles are in the middle lane, and they cannot be detected by the magnetic sensors. Vehicles 3, 5 and 6 are in lane 1 and vehicle 2 is in lane 3. The estimation of these vehicles in the lanes on either side of the road is more accurate, as measured by the normalized innovations, than those in the middle lane. Furthermore, for those vehicles in either side of the road, fusion of both MMW radar and magnetic sensor measurements shows better accuracy than those using MMW radar measurements, while for vehicles in the middle lane, there is no change. The reason is also quite obvious: those in the middle lane cannot be detected by magnetic sensors and therefore cannot enjoy the benefits of data fusion. Therefore Fig. 5 and Table IV allow us to conclude that data fusion not only improve vehicle state estimation in the lateral direction, i.e., the  $y$  coordinate, but also improve the estimation accuracy in the radial direction, i.e., the  $x$  coordinate.

Furthermore, we analyze the effectiveness and rationality of the fusion algorithm using real tunnel scene data. Fig. 6 shows that in the real test, when the vehicle with ID object 53 is driving in lane 1, the radar measurement indicates that the vehicle is in the middle lane. Fig. 7 displays the posterior probability of lane estimation for object 53 based solely on radar measurements. The vehicle is erroneously estimated to be in lane 2 (middle lane) following the update of the 5th, 12th, and 13th inaccurate radar measurements. Subsequently, Fig. 8 demonstrates that fusion with magnetic sensor measurements effectively addresses the issue of incorrect lane estimation caused by inaccurate radar measurements.

To further evaluate the performance before and after the fusion of magnetic sensors when radar measurements are inaccurate, we remove the measurement data of Radar 1 and

TABLE IV  
ROOT MEAN SQUARE OF NORMALIZED INNOVATIONS

Performance	Vehicle 1	Vehicle 2	Vehicle 3	Vehicle 4	Vehicle 5	Vehicle 6
With fusion of both measurements	1.0027	0.4819	0.6316	0.9743	0.5641	0.5843
Using MMW measurements only	1.0027	0.6672	0.8100	0.9743	0.6626	0.7940



Fig. 6. Inaccurate radar measurements of large trucks.

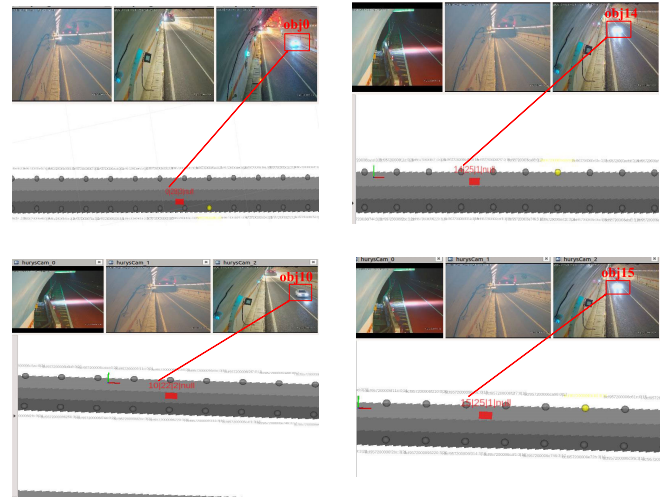


Fig. 9. Tracking performance exhibited by fusion methods in a three-lane tunnel scenario.

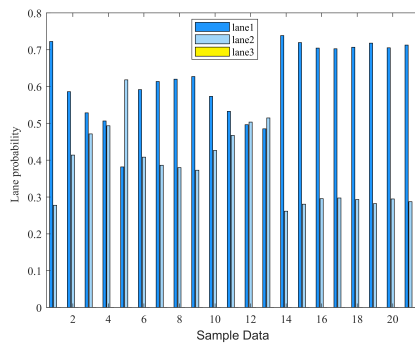


Fig. 7. Lane probability estimates obtained when relying solely on radar measurements. The vehicle is actually driving in lane 1 but may be erroneously estimated to be in lane 2. The system output the lane with the highest probability as the current estimated lane.

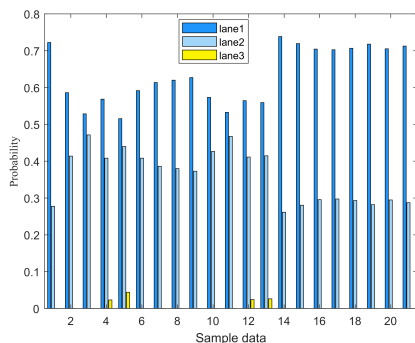


Fig. 8. Lane probability estimates obtained by fusing radar and magnetic sensor measurements when radar measurements are inaccurate. The vehicle is actually driving in lane 1.

Radar 3 and extend the range of interest for Radar 2 and Radar 4 to 300 meters by adjusting the measurement shielding area. This software-based shielding area adjustment ensures that radar measurements beyond the preset detection region of interest (ROI) are not received or used. As mentioned

before, the lateral measurement accuracy of MMW radars decreases sharply with the increase in detection distance. Therefore, by effectively increasing the measurement range of MMW radars from 150 meters to 300 meters, it helps to expose more erroneous measurements of MMW radars and evaluate the effectiveness of magnetic sensor measurement in compensating for MMW measurement errors. Rosbag data recorded every 5-minutes were analyzed. One rosbag packet was randomly selected from all recorded data to compare and analyze the target's trajectory using radar alone and radar-magnetic sensor fusion. Fig. 9 indicates that a 5-minute data packet contains 4 vehicles, observed through the camera: vehicle 14 and vehicle 15 are in lane 1, vehicle 10 is in the middle lane, and vehicle 0 is in lane 3. The same rosbag packet data is executed to compare and analyze vehicle trajectories before and after fusion with magnetic sensors. In Fig. 10, the comparison of trajectory data about position in the  $x$ -direction and  $y$ -direction is shown for the situations of using radars only and combined magnetic sensors and radars, respectively. The blue line represents vehicle tracking solely based on radar output, while the red line represents vehicle tracking using both radars and magnetic sensors. Specifically, vehicle 14 and vehicle 15 in lane 1 are erroneously detected as being in lane 2 by using radar only. However, the vehicle trajectories accurately track vehicles in lane 1 after fused magnetic sensor. Based on the vehicle tracking scenario above, it shown that radar and magnetic sensors have the following advantages: 1) Magnetic sensors help to compensate for the less accurate radial detection of MMW radars; 2) the fusion helps to expand the detection range of MMW radars significantly while maintaining the same level of accuracy.

TABLE V  
PERFORMANCE OF VEHICLE LANE ESTIMATION

Time Period	The number of vehicles with correct lane estimates from radar	The number of vehicles with accurate lane estimates after fusion	Total number of vehicles	Packet time length(min)
2024.1.13-2024.1.20	72	90	90	90
2024.1.21-2024.1.27	90	119	119	115
2024.1.28-2024.2.3	78	98	100	80
2024.2.4-2024.2.10	96	126	126	80

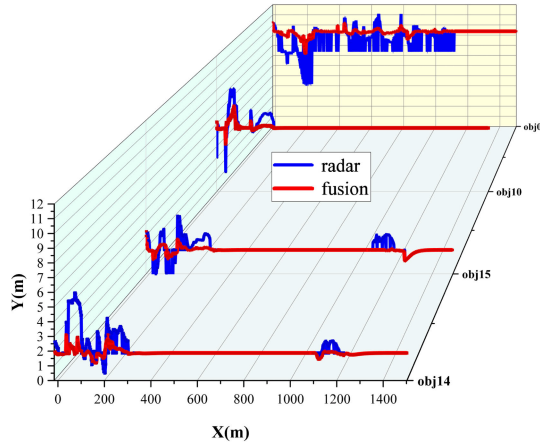


Fig. 10. Trajectory comparison between fused radar and magnetic sensor versus radar-only tracking. The red line represents the combined radar and magnetic sensor tracking, while the blue line represents radar-only tracking.

To further illustrate the complementary advantages of MMW radars and magnetic sensors and quantitatively assess the performance of the proposed algorithm, we record the actual measurement data of the Xianfengding Tunnel and analyze the lane estimation performance. The tracking performance of 435 vehicles recorded during for 365 minutes is summarized in Table V and the ground truth is obtained through manual counting using a video camera. The proposed algorithm with data fusion achieves 99.54% accuracy in the vehicle lane estimation. In contrast, relying solely on radar measurements delivers a lane estimation accuracy of 77.70% only. Additionally, Fig. 11 presents the confusion matrix evaluating lane estimation performance for different sensor combinations. In Fig. 11(a), where only MMW radar is used, the lane estimation accuracies for Lane 1, Lane 2, and Lane 3 are 63.38%, 79.86%, and 80.23%, respectively. In contrast, Fig. 11(b), which incorporates MMW radar and magnetic sensors, shows a significant accuracy improvement of 35.23%, 20.14%, and 18.63% across Lane 1, Lane 2, and Lane 3, respectively, highlighting the advantages of sensor fusion for enhanced vehicle lane estimation. This further confirms the advantage of fusing MMW radars and magnetic sensors. In summary, the proposed fusion method offers several notable advantages: 1) the detection range of MMW radar is significantly expanded while maintaining the same lateral detection accuracy; 2) more reliable and accurate estimation can be obtained both in the lateral direction and in the radial direction; 3) the system with the fusion of radar and magnetic sensors is robust to failure or inaccurate measurements of individual sensors.

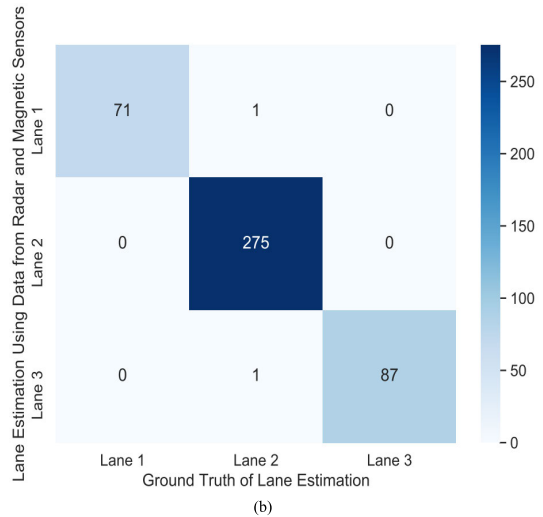
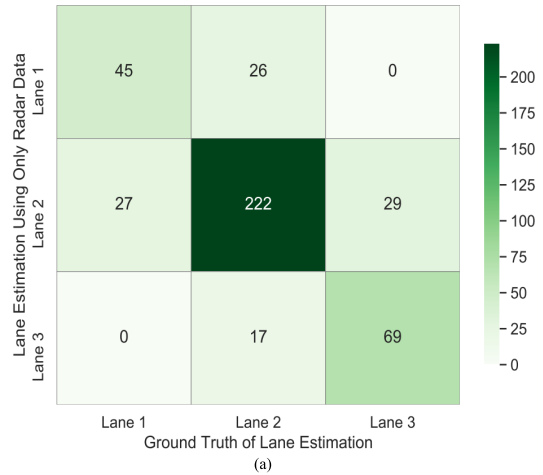


Fig. 11. Performance comparison of lane estimation using different sensor combinations. (a) Confusion matrix for lane estimation using only MMW radar. (b) Confusion matrix for lane estimation obtained from the combination of MMW radar and magnetic sensors.

The total computation time is presented in Table VI. The computing environment was powered by a 11th Gen Intel (R) Core (TM) i7-11700K with 32 GB RAM. The computation times for data association, Kalman filter processing, and lane estimation are 478  $\mu$ s, 445  $\mu$ s, and 227  $\mu$ s, respectively, resulting in a total computation time of 2026  $\mu$ s. Additionally, we also compared the processing times of the fusion center for the entire process from data reception to the completion of state estimation. The calculation times for KF, AKF, AIF and CI were 1749  $\mu$ s, 1954  $\mu$ s, 3850  $\mu$ s, 2276  $\mu$ s, respectively.

TABLE VI  
COMPUTATION TIME

Data process	Data association	Kalman filter	Lane estimation	Total
826 $\mu$ s	478 $\mu$ s	445 $\mu$ s	277 $\mu$ s	2026 $\mu$ s

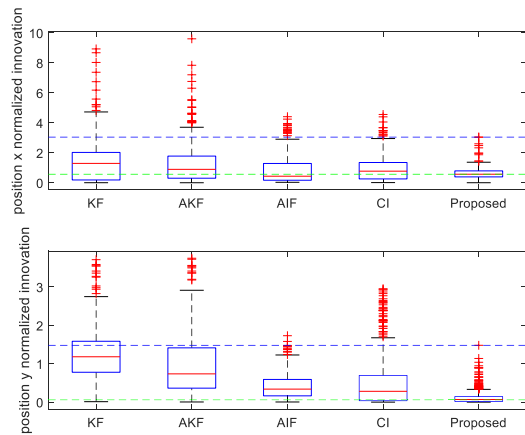


Fig. 12. Comparison of the position normalized innovation for  $x$  and  $y$ . Each box plot illustrates the distribution of the data. The box represents the interquartile range (IQR), which spans from the 25th percentile (lower quartile) to the 75th percentile (upper quartile), while the red line inside the box indicates the median value (50th percentile). The green and blue dashed lines represent the median and maximum values of the proposed algorithm. It can be observed that the proposed algorithm exhibits the smallest maximum error values and minimum median values.

The proposed method demonstrated comparable processing times to these state-of-the-art methods, highlighting its efficiency.

The effectiveness and competitiveness of the proposed algorithm have been validated through experimental comparisons with state-of-the-art methods. Fig.12 presents the comparison results. The normalized innovation values of the Kalman filter (KF) indicate that vehicle tracking in the  $x$ -direction has higher median absolute error, reflecting poor performance due to randomly delayed measurements from the magnetic sensor. In contrast, the proposed algorithm achieves lower maximum error values and exhibits more accurate and stable performance. Unlike the  $x$ -direction, where MMW radar detects vehicles at far distances with significant detection errors, the magnetic sensor mis-detects vehicle lanes in the  $y$ -direction due to interference from vehicles driving in adjacent lane. This suggests that vehicle tracking in the  $y$ -direction has substantial detection uncertainty and estimation error. The bottom part of Fig.12 illustrates tracking performance in the  $y$ -direction. Notably, there is a significant reduction in the normalized innovation and the maximum error in the  $y$ -direction using the proposed method compared to the other methods. The AIF shows suboptimal performance because its matrix-weighted fusion algorithm is capable of handling inaccurate measurements effectively. In contrast, the KF shows the highest median absolute error but with greater instability due to the less accurate lateral measurements from the sensors. Both CI and Method AKF display similar median and maximum absolute error values, indicating comparable performance. In contrast, the proposed method achieves a superior tracking performance in the  $y$ -direction.

This is attributed to the proposed approach of addressing inaccuracies in lateral sensor measurements by modeling the likelihood function using probability density functions and implementing lane-level tracking based on Bayesian weight mixtures.

## VI. CONCLUSION

This work proposed a novel centralized asynchronous fusion method of MMW radars and magnetic sensors for lane-level vehicle tracking. We studied the asynchronous optimal estimation for discrete-time linear system with aperiodic state updating rate and nonuniform measurement sampling rate. Subsequently, Bayesian mixture filtering was employed to estimate the vehicle's lane and achieve lane-level tracking in tunnel with multipath interference, poor light conditions and a lack of satellite signals. Additionally, the proposed fusion method was implemented in a real tunnel and helps to establish a traffic digital twin system for smart tunnel management. Experimental results demonstrated the effectiveness and cost-efficiency of the proposed method based on experiments conducted in Xianfengding Tunnel, Jiangxi, China. Our study provides new insights into roadside sensor fusion.

The good performance of the proposed method, as demonstrated through comprehensive evaluations using both real-world and simulated data, can be attributed to the complementary integration of MMW radar and magnetic sensors, along with the design of a highly robust and accurate fusion algorithm. First, the fusion algorithm significantly expands the detection range of the MMW radar while maintaining the same level of lateral detection accuracy, enabling a broader and more effective sensing capability. Second, the combination of MMW radar and magnetic sensor data provides more reliable and accurate estimations in both the lateral and radial directions. Finally, the system's robustness ensures that it can effectively handle sensor failures or inaccuracies, maintaining high performance even under challenging conditions. These advantages highlight the practical value and reliability of the proposed fusion approach in various scenarios. However, there are still some limitations. For example, the method is not yet capable of accurately detecting abnormal traffic events such as collisions, abnormal stopping, or pedestrian tracking. Future research will focus on the advanced data analysis for real-time and accurate detection of abnormal traffic events such as traffic congestion, abnormal stopping, accidents, and pedestrian tracking.

## APPENDIX A

### ANALYSIS OF GAUSSIAN MIXTURE FUSION WEIGHTS

For an arbitrary probability density function  $f_i(y)$ ,  $i \in \{r, b\}$ , denote the true probability density function by  $p_{true}(y)$ . The true probability density function is generally unknown, and  $f_{fusion}(y)$  is the probability density function that fits the true probability density function  $p_{true}(y)$  after weighted fusion of  $f_i(y)$ ,  $i \in \{r, b\}$ . The KLD of  $p_{true}(y)$  and  $f_{fusion}(y)$  is calculated such that the information loss between the fused probability density function  $f_{fusion}(y)$  and the true probability density function  $p_{true}(y)$  is minimized to determine the

optimal fusion weights, i.e.

$$\begin{aligned}
& D_{KL}(f_{fusion}(y)||p_{true}(y)) \\
&= \int f_{fusion}(y) \log \frac{f_{fusion}(y)}{p_{true}(y)} dy \\
&= \int \sum_{i \in \{r,b\}} \omega_i f_i(y) \log \frac{f_i(y) f_{fusion}(y)}{p_{true}(y) f_i(y)} \delta y \\
&= \sum_{i \in \{r,b\}} \omega_i (D_{KL}(f_i(y)||p_{true}(y)) - D_{KL}(f_i(y)||f_{fusion}(y)))
\end{aligned} \tag{39}$$

where  $\omega_r$  and  $\omega_b$  represent the fusion weights of MMW radar and magnetic sensor, respectively. Following Equation (39), the optimal solution should minimize  $D_{KL}(f_{fusion}(y)||p_{true}(y))$  in order to best the fit true probability density function, i.e

$$\begin{aligned}
\omega_{opt} = \arg \min_w \sum_{i \in \{r,b\}} \omega_i (D_{KL}(f_i(y)||p_{true}(y)) \\
- D_{KL}(f_i(y)||f_{fusion}(y)))
\end{aligned} \tag{40}$$

where  $w = \{\omega_r, \omega_b\}$ .

In practical applications, the true probability density function  $p_{true}(y)$  is unknown, i.e.,  $D_{KL}(f_i(y)||p_{true}(y))$  is unknown. A simple and effective processing method is to convert the minimization problem of Equation (40) into the following constrained maximizing problem [40]:

$$\omega_{subopt} = \arg \max_w \sum_{i \in \{r,b\}} \omega_i (D_{KL}(f_i(y)||f_{fusion}(y))) \tag{41}$$

To solve the optimization problem outlined above and determine the optimal objective function, the formal representation of the problem is as follows:

$$\arg \max_w \sum_{i \in \{r,b\}} \omega_i (D_{KL}(f_i(y)||f_{fusion}(y))) \tag{42}$$

$$s.t. \sum_{i \in \{r,b\}} \omega_i = 1 \tag{43}$$

$$\omega_i \geq 0, i \in \{r, b\} \tag{44}$$

Find the conditional extreme value by constructing Lagrangian function.

$$\begin{aligned}
L(\omega_i, \lambda, a_i) = \sum_{i \in \{r,b\}} \omega_i (D_{KL}(f_i(y)||f_{fusion}(y))) \\
+ \lambda (\sum_{i \in \{r,b\}} \omega_i - 1) + \sum_{i \in \{r,b\}} \omega_i a_i
\end{aligned} \tag{45}$$

where  $\lambda$  and  $a_i$  are the Lagrange multipliers.

The Karush-Kuhn-Tucker (KKT) conditions for the constrained optimization problem are given as follows:

$$\frac{\partial L(\omega_i, \lambda, a_i)}{\partial \omega_i} = 0, i = r, b \tag{46}$$

$$\sum_{i \in \{r,b\}} \omega_i = 1 \tag{47}$$

$$\omega_i \geq 0, i = r, b \tag{48}$$

$$a_i \geq 0, i = r, b \tag{49}$$

$$\omega_i a_i = 0, i = r, b \tag{50}$$

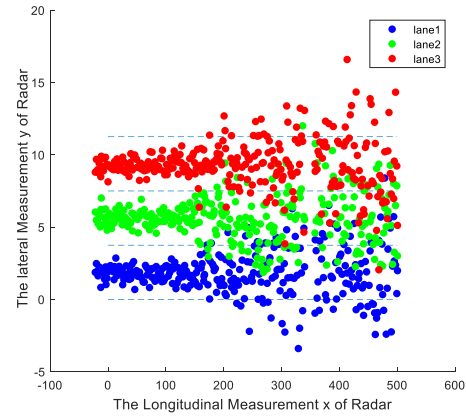


Fig. 13. Simulation of the radar measurements as detection distance increases for vehicles driving in different lanes.

Based on the fusion weights of MMW radar and magnetic sensor obtained by Equation (41)-(50), the fused PDF  $f_{fusion}(y) = \mathcal{N}(u_{fusion}, \delta_{fusion})$  is calculated by arithmetic average (AA) density fusion as follows:

$$f_{fusion}(y) = \omega_r f_r(y) + \omega_b f_b(y) \tag{51}$$

We assume the fused PDF as a single Gaussian, with the mean  $u_{fusion}$  and variance  $\delta_{fusion}$ , calculated from the fusion weights of the MMW radar and magnetic sensor. This assumption is reasonable, as the weighted combination of the Gaussian distributions from both sensors typically results in a distribution that closely approximates a Gaussian, a common approach in many sensor fusion applications. Specifically, the mean and variance are given by:

$$u_{fusion} = \omega_r u_r + \omega_b u_b \tag{52}$$

where  $\omega_r$  and  $\omega_b$  represent the fusion weights of MMW radar and magnetic sensor, respectively, with the constraint  $\omega_r + \omega_b = 1$ .

$$\begin{aligned}
\delta_{fusion} = \omega_r (\delta_r + (u_{fusion} - u_r)(u_{fusion} - u_r)) \\
+ \omega_b (\delta_b + (u_{fusion} - u_b)(u_{fusion} - u_b))
\end{aligned} \tag{53}$$

Finally, the fused probability density function is  $f_{fusion}(y) = \mathcal{N}(u_{fusion}, \delta_{fusion})$ .

## APPENDIX B SIMULATION EVALUATION

The effectiveness and performance of the proposed algorithm are first validated through simulations. As described in Section IV-A, we assume the lane width  $L = 3.75$  meters, Let  $\mu(1) = L/2$ ,  $\mu(2) = 3L/2$ ,  $\mu(3) = 5L/2$  be respectively the centers of Lane 1, Lane 2 and Lane 3 along the  $y$  axis. The initial detected vehicle positions  $(z_x(0), z_y(0))$  in three lanes are  $(0, 1.875)$ ,  $(0, 5.625)$ ,  $(0, 9.375)$ , respectively. When the measurement distance is less than 150 meters, the angle measurement error is set to  $\delta_\theta = 0.0052rad$ . When the distance is greater than 150 meters, the angle measurement error  $\delta_\theta = 0.0017rad$ . The MMW radar's distance measurement error is  $\delta = 0.2$ . The threshold of 150 meters was established through empirical measurements from real-world MMW radar deployments, specifically during the on-site

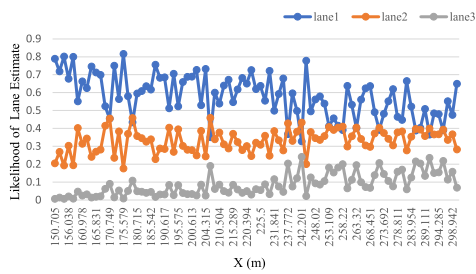


Fig. 14. The likelihood of lane estimates for a vehicle driving in Lane 1 and at a distance of 150-300 meters away from the radar using radar measurements only.

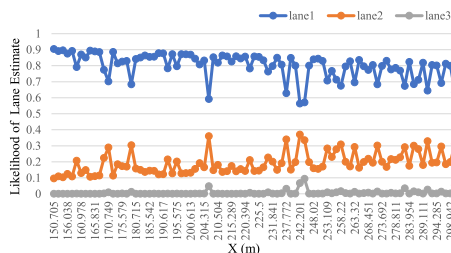


Fig. 15. The likelihood of lane estimates for a vehicle driving in Lane 1 and at a distance of 150-300 meters away from the radar using fused measurements from both the radars and the magnetic sensors.

calibration of MMW radar in a tunnel environment. Then, the measurement error in the  $y$ -direction at close range ( $r < 150$ ) can be approximated by  $\delta_r^2 = r^2 \delta_\theta^2 = (0.0052)^2 r^2$ . The measurement error in the  $y$ -direction at far range ( $r > 150$ ) can be  $\delta_r^2 = r^2 \delta_\theta^2 z_x^2 / r^2 + \delta_z^2 z_y^2 / r^2$ . The measurement noise of the radar in the  $y$ -direction can be assumed to be  $n_y \sim N(0, \delta_r)$ . The simulated measurement data generated by the radar in the  $y$ -direction can be  $z_y(k) = z_y(k-1) + n_y$ . The sampling period is 0.1 s. The vehicle is assumed to move at a constant velocity in the  $x$ -direction, advancing 2 meters each sampling period. The simulation runs for 250 time steps. Fig. 13 shows simulated radar measurement data. As expected, radar measurements exhibit inaccurate lateral detection as the detection distance increases. Within the detection range of 0 to 150 meters, radar measurements can accurately capture the lane in which the vehicle is driving. However, beyond approximately 150 meters, radar measurements become inaccurate.

Scenario 1: Inaccurate radar measurements occur at far distances.

Fig. 14 shows the likelihood of lane estimates for a vehicle driving in Lane 1 and at a distance of 150-300 meters away from the radar using radar measurements only, where the likelihood function is obtained from radar measurements using (31), (32) and (33). As shown in Fig. 14, there are several instances where the vehicle is incorrectly estimated to be in Lane 2, based solely on radar measurements. In comparison, Fig. 15 displays the likelihood of lane estimates under the same conditions, but with fused measurements from MMW radars and magnetic sensors. The results in Fig. 15 shows apparent improvement in the lane estimation accuracy. Due to the deployment pattern of magnetic sensors, the detection accuracy along the  $y$  axis of magnetic sensors is unaffected by the vehicle's position along the  $x$  axis. This advantage complements the weakness in radar detection that the lateral detection accuracy deteriorates with the detection distance.

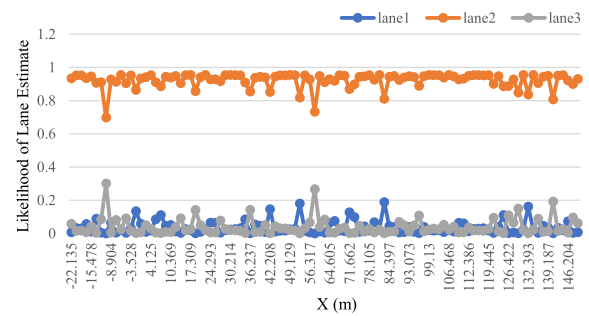


Fig. 16. The likelihood of radar in the 0-150m detection range when the vehicle is in the middle lane.

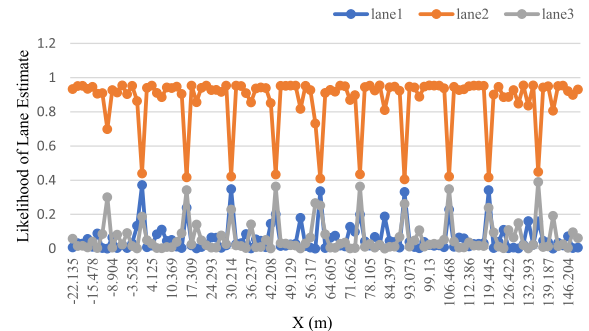


Fig. 17. The likelihood of fusing magnetic sensors and radar within the 0-150m detection range when the vehicle is in the middle lane.

Scenario 2: False detection from adjacent lane vehicles by magnetic sensors (vehicle is in the middle lane, magnetic sensors on both sides are falsely triggered)

Fig. 16 illustrates that relying solely on radar within the 0-150 meters detection range accurately reflects the vehicle in the middle lane. However, when a vehicle is in the middle lane, the magnetic sensors deployed in lane lines 0 and 3 on both sides of the lane will generally not be triggered unless adjacent lane vehicle false detection occasionally occurs, causing them to be mistakenly detected. The likelihood after fusing the magnetic sensors and radar is depicted in Fig. 17. Despite the reduction in radar likelihood, it still indicates the vehicle is in the middle lane. This mainly takes advantage of radar's superior detection capabilities at close distance, resulting in a large fusion weight for radar compared to the magnetic sensor, consistent with our theoretical expectations.

Simulation studies confirm the effectiveness of the MMW radar and the magnetic sensor fusion in improving the accuracy of the lane estimates. Extensive simulation tests have been conducted which shows the superiority of data fusion of the MMW radars and the magnetic sensors, not only in improving the accuracy and robustness of lane estimates but also an overall improvement in vehicle tracking performance.

## REFERENCES

- [1] G. Mao, Y. Hui, X. Ren, C. Li, and Y. Shao, "The Internet of Things for smart roads: A road map from present to future road infrastructure," *IEEE Intell. Transp. Syst. Mag.*, vol. 14, no. 6, pp. 66–76, Nov. 2022.
- [2] Q. Wang, J. Zheng, H. Xu, B. Xu, and R. Chen, "Roadside magnetic sensor system for vehicle detection in urban environments," *IEEE Trans. Intell. Transp. Syst.*, vol. 19, no. 5, pp. 1365–1374, May 2018.
- [3] P. Liu, G. Yu, Z. Wang, B. Zhou, and P. Chen, "Object classification based on enhanced evidence theory: Radar-vision fusion approach for roadside application," *IEEE Trans. Instrum. Meas.*, vol. 71, pp. 1–12, 2022.

- [4] Y. Du, B. Qin, C. Zhao, Y. Zhu, J. Cao, and Y. Ji, "A novel spatio-temporal synchronization method of roadside asynchronous MMW radar-camera for sensor fusion," *IEEE Trans. Intell. Transp. Syst.*, vol. 23, no. 11, pp. 22278–22289, Nov. 2022.
- [5] S. Wang et al., "Object tracking based on the fusion of roadside LiDAR and camera data," *IEEE Trans. Instrum. Meas.*, vol. 71, pp. 1–14, 2022.
- [6] X. Han et al., "Foundation intelligence for smart infrastructure services in transportation 5.0," *IEEE Trans. Intell. Vehicles*, vol. 9, no. 1, pp. 39–47, Jan. 2024.
- [7] R. Zhang, D. Meng, L. Bassett, S. Shen, Z. Zou, and H. X. Liu, "Robust roadside perception: An automated data synthesis pipeline minimizing human annotation," 2023, *arXiv:2306.17302*.
- [8] C. Ounoughi and S. Ben Yahia, "Data fusion for ITS: A systematic literature review," *Inf. Fusion*, vol. 89, pp. 267–291, Jan. 2023.
- [9] K. Shen, Y. Li, T. Liu, J. Zuo, and Z. Yang, "Adaptive-robust fusion strategy for autonomous navigation in GNSS-challenged environments," *IEEE Internet Things J.*, vol. 11, no. 4, pp. 6817–6832, Feb. 2024.
- [10] E. Arnold, M. Dianati, R. de Temple, and S. Fallah, "Cooperative perception for 3D object detection in driving scenarios using infrastructure sensors," *IEEE Trans. Intell. Transp. Syst.*, vol. 23, no. 3, pp. 1852–1864, Oct. 2020.
- [11] R. Chen, L. Gao, Y. Liu, Y. L. Guan, and Y. Zhang, "Smart roads: Roadside perception, vehicle-road cooperation and business model," 2023, *arXiv:2312.09439*.
- [12] Z. Liu et al., "Robust target recognition and tracking of self-driving cars with radar and camera information fusion under severe weather conditions," *IEEE Trans. Intell. Transp. Syst.*, vol. 23, no. 7, pp. 6640–6653, Jul. 2022.
- [13] C. Chen, S. Rosa, C. X. Lu, B. Wang, N. Trigoni, and A. Markham, "Learning selective sensor fusion for state estimation," *IEEE Trans. Neural Netw. Learn. Syst.*, pp. 1–15, 2022.
- [14] C. Tu, E. Takeuchi, A. Carballo, C. Miyajima, and K. Takeda, "Motion analysis and performance improved method for 3D LiDAR sensor data compression," *IEEE Trans. Intell. Transp. Syst.*, vol. 22, no. 1, pp. 243–256, Jan. 2021.
- [15] J. Shi, G. Hu, X. Zhang, and F. Sun, "Sparsity-based DOA estimation of coherent and uncorrelated targets with flexible MIMO radar," *IEEE Trans. Veh. Technol.*, vol. 68, no. 6, pp. 5835–5848, Jun. 2019.
- [16] K. Wang, H. Xiong, J. Zhang, H. Chen, D. Dou, and C.-Z. Xu, "SenseMag: Enabling low-cost traffic monitoring using noninvasive magnetic sensing," *IEEE Internet Things J.*, vol. 8, no. 22, pp. 16666–16679, Nov. 2021.
- [17] A. Amodio, M. Ermidoro, S. M. Savaresi, and F. Previdi, "Automatic vehicle model recognition and lateral position estimation based on magnetic sensors," *IEEE Trans. Intell. Transp. Syst.*, vol. 22, no. 5, pp. 2775–2785, May 2021.
- [18] Y. Feng, J. A. Zhang, B. Cheng, X. He, and J. Chen, "Magnetic sensor-based multi-vehicle data association," *IEEE Sensors J.*, vol. 21, no. 21, pp. 24709–24719, Nov. 2021.
- [19] Z. Zhang, X. Mao, K. Zhou, and H. Yuan, "Collaborative sensing-based parking tracking system with wireless magnetic sensor network," *IEEE Sensors J.*, vol. 20, no. 9, pp. 4859–4867, May 2020.
- [20] Y. Feng et al., "MagMonitor: Vehicle speed estimation and vehicle classification through a magnetic sensor," *IEEE Trans. Intell. Transp. Syst.*, vol. 23, no. 2, pp. 1311–1322, Feb. 2022.
- [21] D. J. Yeong, G. Velasco-Hernandez, J. Barry, and J. Walsh, "Sensor and sensor fusion technology in autonomous vehicles: A review," *Sensors*, vol. 21, no. 6, p. 2140, Mar. 2021.
- [22] Y. Hu, Z. Duan, and D. Zhou, "Estimation fusion with general asynchronous multi-rate sensors," *IEEE Trans. Aerosp. Electron. Syst.*, vol. 46, no. 4, pp. 2090–2102, Oct. 2010.
- [23] L. Yan, X. R. Li, Y. Xia, and M. Fu, "Modeling and estimation of asynchronous multirate multisensor system with unreliable measurements," *IEEE Trans. Aerosp. Electron. Syst.*, vol. 51, no. 3, pp. 2012–2026, Jul. 2015.
- [24] W. D. Blair, T. R. Rice, A. T. Alouani, and P. Xia, "Asynchronous data fusion for target tracking with a multitasking radar and optical sensor," *Proc. SPIE*, vol. 1482, pp. 234–245, Aug. 1991.
- [25] C. Zhai, M. Wang, Y. Yang, and K. Shen, "Robust vision-aided inertial navigation system for protection against ego-motion uncertainty of unmanned ground vehicle," *IEEE Trans. Ind. Electron.*, vol. 68, no. 12, pp. 12462–12471, Dec. 2021.
- [26] S. Sun, H. Lin, J. Ma, and X. Li, "Multi-sensor distributed fusion estimation with applications in networked systems: A review paper," *Inf. Fusion*, vol. 38, pp. 122–134, Nov. 2017.
- [27] Q. Liu, Z. Wang, X. He, and D. H. Zhou, "On Kalman-consensus filtering with random link failures over sensor networks," *IEEE Trans. Autom. Control*, vol. 63, no. 8, pp. 2701–2708, Aug. 2018.
- [28] X. Hao, Y. Xia, H. Yang, and Z. Zuo, "Asynchronous information fusion in intelligent driving systems for target tracking using cameras and radars," *IEEE Trans. Ind. Electron.*, vol. 70, no. 3, pp. 2708–2717, Mar. 2023.
- [29] K. Cai, T. Qu, H. Chen, B. Gao, and N. Bian, "Low-cost hybrid multisensor fusion method and implementation for production intelligent vehicles," *IEEE Trans. Instrum. Meas.*, vol. 71, pp. 1–16, 2022.
- [30] Y. Shen, Z. Wang, H. Dong, and H. Liu, "Multi-sensor multi-rate fusion estimation for networked systems: Advances and perspectives," *Inf. Fusion*, vol. 82, pp. 19–27, Jun. 2022.
- [31] H. Lin and S. Sun, "Estimator for multirate sampling systems with multiple random measurement time delays," *IEEE Trans. Autom. Control*, vol. 67, no. 3, pp. 1589–1596, Mar. 2022.
- [32] H. Lin and S. Sun, "An overview of multirate multisensor systems: Modelling and estimation," *Inf. Fusion*, vol. 52, pp. 335–343, Dec. 2019.
- [33] W.-A. Zhang, M. Z. Q. Chen, A. Liu, and S. Liu, "Aperiodic optimal linear estimation for networked systems with communication uncertainties," *IEEE Trans. Cybern.*, vol. 47, no. 8, pp. 2256–2265, Aug. 2017.
- [34] H. Lin and S. Sun, "Estimation for networked random sampling systems with packet losses," *IEEE Trans. Syst. Man, Cybern. Syst.*, vol. 51, no. 9, pp. 5511–5521, Sep. 2021.
- [35] Y. Bar-Shalom, "Update with out-of-sequence measurements in tracking: Exact solution," *IEEE Trans. Aerosp. Electron. Syst.*, vol. 38, no. 3, pp. 769–777, Jul. 2002.
- [36] J. Kim, K. Jo, W. Lim, M. Lee, and M. Sunwoo, "Curvilinear-coordinate-based object and situation assessment for highly automated vehicles," *IEEE Trans. Intell. Transp. Syst.*, vol. 16, no. 3, pp. 1559–1575, Jun. 2015.
- [37] K. Jo, M. Lee, and M. Sunwoo, "Track fusion and behavioral reasoning for moving vehicles based on curvilinear coordinates of roadway geometries," *IEEE Trans. Intell. Transp. Syst.*, vol. 19, no. 9, pp. 3068–3075, Sep. 2018.
- [38] V. K. Shopov and V. D. Markova, "Application of Hungarian algorithm for assignment problem," in *Proc. Int. Conf. Inf. Technol. (InfoTech)*, Sep. 2021, pp. 1–4.
- [39] S. S. Blackman and R. Popoli, "Design and analysis of modern tracking systems," Tech. Rep., 1999.
- [40] T. Li, H. Liang, B. Xiao, Q. Pan, and Y. He, "Finite mixture modeling in time series: A survey of Bayesian filters and fusion approaches," *Inf. Fusion*, vol. 98, Oct. 2023, Art. no. 101827.
- [41] T. Van Erven and P. Harremoos, "Rényi divergence and Kullback–Leibler divergence," *IEEE Trans. Inf. Theory*, vol. 60, no. 7, pp. 3797–3820, Jun. 2014.
- [42] Y. Bar-Shalom, P. K. Willett, and X. Tian, *Tracking Data Fusion*, vol. 11. Storrs, CT, USA: YBS Publishing, 2011.
- [43] Y. Song, Z. Hu, T. Li, and H. Fan, "Performance evaluation metrics and approaches for target tracking: A survey," *Sensors*, vol. 22, no. 3, p. 793, Jan. 2022.
- [44] J. García, J. M. Molina, and J. Trincado, "Real evaluation for designing sensor fusion in UAV platforms," *Inf. Fusion*, vol. 63, pp. 136–152, Nov. 2020.



**Guoqiang Mao** (Fellow, IEEE) was a Leading Professor, the Founding Director of the Research Institute of Smart Transportation, and the Vice-Director of the ISN State Key Laboratory, Xidian University, from 2014 to 2019. Before that, he was with the University of Technology Sydney and the University of Sydney. He is currently a Chair Professor and the Director of the Center for Smart Driving and Intelligent Transportation Systems, Southeast University. He has published 300 papers in international conferences and journals that have been cited more than 15 000 times. His H-index is 57. His research interests include intelligent transport systems, the Internet of Things, wireless localization techniques, mobile communication systems, and applied graph theory and its applications in telecommunications. He is a fellow of AAAI and IET. He received the "Top Editor" Award for outstanding contributions to IEEE TRANSACTIONS ON VEHICULAR TECHNOLOGY in 2011, 2014, and 2015. He was the Co-Chair

of the IEEE ITS Technical Committee on Communication Networks (2014–2017). He has served as the chair, the co-chair, and a TPC member in a number of international conferences. He has been serving as the Vice-Director for the Smart Transportation Information Engineering Society, Chinese Institute of Electronics, since 2022, and an Editor of IEEE TRANSACTIONS ON INTELLIGENT TRANSPORTATION SYSTEMS since 2018. He was an Editor of IEEE TRANSACTIONS ON WIRELESS COMMUNICATIONS (2014–2019) and IEEE TRANSACTIONS ON VEHICULAR TECHNOLOGY (2010–2020). He is on the list of Top 2% most-cited Scientists Worldwide by Stanford University in 2022, 2023, and 2024 both by Single Year and by Career Impact.



**Tianxuan Fu** received the master's degree in transport information engineering and control from Lanzhou Jiaotong University, Lanzhou, China, in 2019. He is currently pursuing the Ph.D. degree with the College of Communication Engineering, Xidian University, Xi'an, China. His research interests include target tracking, data fusion, and intelligent transportation systems.



**Xiaojiang Ren** (Member, IEEE) received the Ph.D. degree in computer science from The Australian National University in 2016. He is currently an Associate Professor with Xidian University, Xi'an, China. His research interests include intelligent transport systems, the Internet of Things, wireless sensor networks, routing protocol design for wireless networks, and optimization problems.



**Keyin Wang** (Graduate Student Member, IEEE) received the master's degree in control engineering from Hubei University of Automotive Technology, Shiyan, China, in 2022. He is currently pursuing the Ph.D. degree with the College of Communication Engineering, Xidian University, Xi'an, China. His research interests include vehicle localization based on multisource information fusion.



**Zhaozhong Zhang** received the B.E. degree from the University of Nottingham, U.K., in 2013, and the M.S. and Ph.D. degrees in automotive engineering and transport systems from Cranfield University, U.K., in 2015 and 2020, respectively. He is currently a Lecturer with the School of Information Engineering, Nanchang Hangkong University. His research interests include vehicle localization and target tracking.



**Zhong Wu** received the master's degree in computer science and technology from Nanchang University of Aeronautics and Astronautics. He was the General Manager and a Senior Engineer of Beijing Zhongrui Fangxing Technology Company Ltd., a subsidiary of Jiangxi Xixing Technology Company Ltd. His main research interests include highway electromechanical informatization and intelligent traffic perception products and solutions.



**Dahai Xu** received the degree from Jiangxi Institute of Science and Technology, China, in 2012, and the master's degree in control engineering from Nanchang University. He is currently the Manager of the Product Research and Development Department, Beijing Zhongrui Fangxing Technology Company Ltd. His research interests include intelligent control of highways and intelligent transportation terminal products.